Geophys. J. Int. (2007) **168,** 1175–1194 doi: 10.1111/j.1365-246X.2006.03251.x

Earthquake spatial distribution: the correlation dimension

Yan Y. Kagan

Department of Earth and Space Sciences, University of California, Los Angeles, CA 90095-1567*, USA. E-mail: ykagan@ucla.edu*

Accepted 2006 September 28. Received 2006 September 27; in original form 2006 January 6

SUMMARY

We review methods for determining the fractal dimensions of earthquake epicentres and hypocentres, paying special attention to the problem of errors, biases and systematic effects. Among effects considered are earthquake location errors, boundary effects, inhomogeneity of depth distribution and temporal dependence. In particular, the correlation dimension of earthquake spatial distribution is discussed, techniques for its evaluation presented, and results for several earthquake catalogues are analysed. We show that practically any value for the correlation dimension can be obtained if many errors and inhomogeneities in observational data as well as deficiencies in data processing are not properly considered. It is likely that such technical difficulties are intensified when one attempts to evaluate multifractal measures of dimension. Taking into account possible errors and biases, we conclude that the fractal dimension for shallow seismicity asymptotically approaches 2.20 ± 0.05 for a catalogue time span of decades and perhaps centuries. The value of the correlation dimension declines to 1.8–1.9 for intermediate events (depth interval 71–280 km) and to 1.5–1.6 for deeper ones.

Key words: earthquake location, fractals, geostatistics, seismicity, statistical methods, synthetic-earthquake catalogues.

1 INTRODUCTION

This paper continues our research into spatial patterns of earthquake occurrence (Kagan & Knopoff 1978, 1980; Kagan 1981a,b, 1991a). In the last 5–10 yr many papers (see below) have been published which analysed both theoretical and phenomenological aspects of the scale-invariant spatial features of earthquakes. Various values for scaling exponents have been proposed. However, it is not clear whether such diversity is due to real physical reasons or is caused by data deficiencies and failure to consider the properties of earthquake process.

In this paper, we analyse the statistical distributions of earthquake epicentres and hypocentres. Since this distribution exhibits scale-invariant properties, it is often called a fractal spatial distribution (Kagan & Knopoff 1978, 1980; Ogata & Katsura 1991; Kagan 1991a; Harte 1998, 2001; Vere-Jones 1999; Bak *et al.* 2002) and is characterized by its fractal and, in particular, correlation dimension, δ. Several sources of random and systematic errors as well as biases in the dimension determination need to be considered first.

As a major tool in this study, we analyse a distribution of distances between any event pairs in several earthquake catalogues. Thus, we study the correlation dimension of earthquake spatial patterns. Studying distances has a certain advantage compared to the widely used box-counting methods for studying fractal patterns. For example, southern California seismicity exhibits clear alignment along the plate boundaries and the San Andreas fault system. It is possible, therefore, that cells oriented along the fault would yield a different result compared to boxes selected along latitude/longitude lines. In addition, the initial grid location and the size of the smallest and largest cells can influence the box-counting algorithm (Molchan & Kronrod 2005).

The distances between events do not depend, as boxes do, on the system coordinates and the grid selection. Moreover, distances can be defined on a surface of a 2-D sphere. Box-counting on a spherical surface, when analysis is extended over large spherical regions, cannot be used without unknown modifications at present. This is perhaps one reason why box-counting techniques have been employed in relatively limited seismic regions like California (Geilikman *et al.* 1990; Bak *et al.* 2002; Molchan & Kronrod 2005).

As we will see, investigating local catalogues presents serious problems connected with boundary effects and the high spatial inhomogeneity of the location accuracy and magnitude threshold. These drawbacks are largely due to the spatial boundaries of the catalogues, and are especially strong for networks situated on island chains like Japan and New Zealand where station distribution is almost 1-D. Therefore, we should compare results for local or regional catalogues with studies of global earthquake catalogues in which the above problems are significantly alleviated.

For example, Harte & Vere-Jones (1999) paired up the events listed in the PDE and New Zealand catalogues and studied the difference in the tabulated solutions. They found that earthquake epicentres in some regions are systematically displaced in one catalogue relative to another, and earthquake depths are often also systematically different. This effect is a natural consequence of

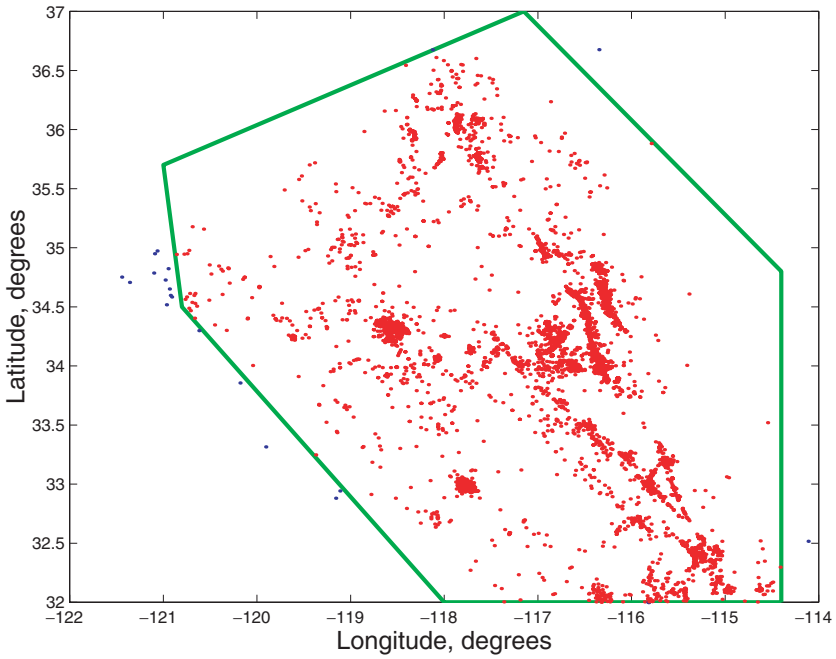

Figure 1. Epicentre distribution of earthquakes in southern California in the Hauksson & Shearer (2005) catalogue. Time interval is 1984–2002, magnitude threshold $M_c = 3$. A 6-point box with the following coordinates is used: North latitude—32.0°, 34.8°, 37.0°, 35.7°, 34.5° and 32.0°; West longitude—114.4°, 114.4°, 117.15°, 121.0°, 120.8° and 118.0°. Earthquake distribution is considered to be reasonably homogeneous and complete in this box for the CalTech catalogue (L. M. Jones, private communication, 2002). The area of the box is $S \approx 233\,300$ km^2.

different station distribution in these catalogues, as well as different interpretation methods. However, for global catalogues one should expect less variation in location bias, and since in this work we are not interested in real earthquake locations but in distances between catalogue solutions, global catalogues may have certain advantages compared to local ones.

In particular, we are interested here primarily in the *hypocentral* fractal pattern, since this pattern characterizes physical properties of the earthquake rupture process. However, in many earthquake catalogues, unreliable source depth information forces one to study epicentral distribution. Moreover, seismicity is usually concentrated in the upper crust, corresponding to a narrow layer of 15–20 km thickness. For distances exceeding that width, epicentral and hypocentral moments converge (Section 5). Therefore, we consider the interrelationship between these two distributions and show how the epicentral fractal pattern can be used to infer the value of the hypocentral correlation dimension, especially for large distances.

For distances comparable to the seismogenic depth interval, the epicentral distribution may be strongly influenced by projection effects which increase the estimate of the correlation dimension for a set of epicentres. We calculate appropriate corrections so that the biases can be more accurately estimated. Similarly, the hypocentral moment function changes significantly when calculated for a seismogenic layer at distances comparable to or exceeding its thickness.

In most studies of earthquake spatial distribution, location and other errors have not been properly considered. This oversight might explain the high values of fractal dimensions often reported and their great variability, findings which do not reflect the physical and geometrical properties of the earthquake fracture but rather indicate location and projection errors peculiar to the catalogues studied.

The notable feature of the present investigation is its emphasis on analysis of the errors and systematic effects in studying the correlation dimension. As we show, these effects are often so large that they may render the results of any statistical analysis irrelevant, if these influences are not noted.

In Fig. 1, we show epicentres in the catalogue compiled by Hauksson & Shearer (2005) (see Section 3 below) for the period 1984–2002. The accuracy of the hypocentre location is very high; in many cases the errors do not exceed 0.1 km. For the faults that are vertical or close to vertical, such as the 1992 Landers (coordinates 34.20°N, 116.44°W—see Kagan *et al.* 2006) or the 1999 Hector Mine (34.59°N, 116.27°W) earthquakes, the epicentres delineate the major faults as well as subsidiary features. However, for the 1994 Northridge earthquake (34.21°N, 118.54°W), epicentres form a cloud. This happens because the rupture plane of the earthquake was far from vertical (Thio & Kanamori 1996).

We can compare Fig. 1 with the epicentre maps for the local catalogue for southern California for 1800–2005 (see Kagan *et al.* 2006). This catalogue combines historical and instrumental earthquake catalogues. Several features can be seen in that catalogue: although most aftershocks of the 1857 Fort Tejon earthquake are likely to be missing, and the location accuracy is low for historic earthquakes, the spatial distribution is more uniform along the San Andreas fault than similar distributions are for the catalogues of a more limited time span.

The earthquakes in Fig. 1 show strong concentration in a few clusters, often connected to the aftershock sequences of strong events. This narrow clustering, as we will see, leads to a decrease in the correlation dimension of earthquake distribution. On the other hand, the broad earthquake distribution such as fig. 1 in Kagan *et al.* (2006) produces a larger value of that dimension.

Describing scale-invariant point patterns, like that shown in Fig. 1, presents serious methodological and theoretical problems, since the mathematical framework for analysis is not yet completed. The first

approach is to treat this pattern as a stochastic point process (Vere-Jones 1999; Daley & Vere-Jones 2003). For such a process the covariance measure C_2 can be defined by

$$C_2(y-x) \;=\; m\,[\,m_1(y|x) - m\,], \tag{1}$$

where m is a point mean density, and the conditional first moment measure or the Palm intensity $m_1(y|x)$ is a function of distance $y - x$ (Kagan & Vere-Jones 1996). Moment m_1 is proportional to the number of event pairs at various distance intervals measured for each point. In the earthquake applications, when $m_1(y|x) \gg m$ for $y - x$ small, it is probably impossible to determine from a finite data set, whether the power decay relates to $m_1(y|x)$ directly, or to the difference $m_1(y|x) - m$. For fractal distributions the moment m_1 has a power-law dependence on distance R

$$m_1(R) \;\propto\; R^{\delta-1}. \tag{2}$$

Another approach is to use total counts of point pairs in the analysis as they depend on their distance. This is usual treatment of fractal point patterns whether they are encountered in *phase space* of strange attractors (see e.g. Nerenberg & Essex 1990; Harte 2001) or in *real space* of earthquake spatial distribution. In this work, depending on dimensionality D of the space considered, we study the total number of earthquake pairs at distance R

$$N_D(R) \;\propto\; R^{\delta}. \tag{3}$$

Then the simplest estimate of $\hat{\delta}$ is a straight line in a log–log plot N_D versus R, or

$$\hat{\delta} \;=\; \frac{\partial\,[\log N_D(R)]}{\partial\,(\log R)}. \tag{4}$$

Because of different mathematical tools used in the analysis of point patterns, the terminology is not yet stabilized. This is the reason that in various papers (including ours) different terms (like statistical moments or pair numbers, see eqs 2 and 3) sometimes are employed to describe the earthquake spatial patterns.

2 SIMULATING POINT SPATIAL PATTERNS

Simulating spatial distributions is often necessary in testing formulae to estimate various dimensions of point patterns and different biases caused by location errors and other defects in earthquake data (see Section 4 below).

The non-fractal point distribution can be simulated by placing points randomly in a region of a 2-D plane or 3-D volume. The resulting point pattern is a spatial Poisson process. Ripley (1988) and Stoyan & Stoyan (1994) discuss these simulations in more detail.

To simulate random points in a window in a sphere with longitude limits x_1 and x_2 and latitude limits y_1 and y_2, we use the following formula

$$\begin{aligned} x &= x_1 + Z_1 \times (x_2 - x_1), \quad \text{and} \\ y &= \arcsin[Z_2 \times (\sin(y_2) - \sin(y_1)) + \sin(y_1)], \end{aligned} \tag{5}$$

where Z_i are uniformly distributed random numbers in a range (0, 1].

To create a point pair for a fractal point pattern, we use Lévy flight pattern (Mandelbrot 1983). We put one point at the centre and use the truncated Pareto distribution to simulate the position of a second. The probability density function for the distance r is

$$\phi(r) \;=\; \frac{r_{\max}^{\delta}\, r_{\min}^{\delta}}{r_{\max}^{\delta} - r_{\min}^{\delta}}\,\delta\, r^{-1-\delta} \quad \text{for} \quad r_{\min} \le r \le r_{\max}, \tag{6}$$

and the distribution function

$$\Phi(r) \;=\; \frac{(r_{\min}/r)^{\delta} - (r_{\min}/r_{\max})^{\delta}}{1 - (r_{\min}/r_{\max})^{\delta}} \quad \text{for} \quad r_{\min} \le r \le r_{\max}, \tag{7}$$

where $r_{\min}$ and $r_{\max}$ are the minimum and maximum distances, and δ is the dimension of the pattern.

For the truncated Pareto distribution, we simulate distances as

$$r \;=\; r_{\min}\left\{Z\left[1 - (r_{\max}/r_{\min})^{-\delta}\right] + (r_{\max}/r_{\min})^{-\delta}\right\}^{-1/\delta}, \tag{8}$$

where Z is the same as in (5). The random point is then obtained by simulating a normalized random 3-D vector with Marsaglia's (1972) algorithm (see also http://mathworld.wolfram.com/SpherePointPicking.html) and putting a point along the vector at the distance r.

The simulation methods described above have two disadvantages. The points can be too orderly (e.g. the pattern of random points on a 2-D plane or spherical surface as in eq. 5). Or with the other simulation technique (6–8), a direction from one random point to another is isotropically distributed in a 3-D space but accounts for position of no other points. Earthquake point patterns clearly deviate from planar geometry: earthquake faults branch and form en-echelon patterns and other complex shapes (Kagan 1991a; Ben-Zion & Sammis 2003). On the other hand, the fractal point structure exhibits obvious anisotropy (Kagan 1981a;b); linear features in 2-D and planar in 3-D are good approximations. Kagan (1982) and Libicki & Ben-Zion (2005) created models of earthquake fault geometry that try to capture such features. However, here we use only simple geometrical patterns (eqs 5–8). Therefore, our derived corrections for the biases and other deficiencies of earthquake catalogues should be considered a first approximation.

3 EARTHQUAKE CATALOGUES

Beginning in 1932, the CalTech (CIT) data set (Hileman *et al.* 1973; Hutton & Jones 1993) was the first instrumental local catalogue to include small earthquakes ($M \ge 3$). In recent years even smaller earthquakes have been included in the catalogue. Presently the magnitude threshold is about 1.5 (Wiemer & Wyss 2000).

The catalogue of relocated earthquakes (Richards-Dinger & Shearer 2000) contains 297 400 events for the period 1975–1998. These events have been relocated using spatially varying station terms to improve the accuracy of relative location. The median horizontal accuracy is 0.3 km and the vertical uncertainty is about 0.7 km. These values are significantly better then those for the CIT catalogue, especially during its early period.

Another relocated catalogue for southern California was produced by Hauksson & Shearer (2005) and Shearer *et al.* (2005). They applied waveform cross-correlation to obtain precise differential times between nearby events. These times can then be used to greatly improve the relative location accuracy within clusters of similar events. In many regions, this new catalogue resolves individual faults in what previously appeared to be diffuse earthquake clouds (see figs 1 and 7 in Shearer *et al.* 2005).

Richards *et al.* (2006) compare traditional methods of earthquake location and discuss the advantages of modern location methods and their application for California catalogues. They show that for these new methods the location uncertainty is 10–100 times lower than for old catalogues based on seismic phase pick data.

The Preliminary Determination of Epicentres (PDE, 1999, and references therein) worldwide catalogue is issued by the USGS

(U.S. Geological Survey). The catalogue contains more than 50 000 shallow earthquakes with $m_b \geq 5$ from 1965 to 2004/1/1.

4 SOURCES OF ERROR AND BIAS IN ESTIMATING THE CORRELATION DIMENSION

There is an extensive bibliography on statistical estimation of the dimension (e.g., Smith 1988; Nerenberg & Essex 1990; Ogata & Katsura 1991; Pisarenko & Pisarenko 1995; Eneva 1996; Vere-Jones *et al.* 1997; Harte 1998, 2001; De Luca *et al.* 1999, 2002; Vere-Jones 1999; Molchan & Kronrod 2005 and references therein). However, these publications insufficiently consider the systematic effects which largely influence estimation of the fractal or scaling dimensions for earthquakes. Many of these publications consider methods for estimating correlation dimension with little quantitative discussion of various biases, which as we see later, may significantly alter the dimension value even if evaluated by a seemingly efficient statistical method. Some of the above publications estimated several effects using synthetic catalogues. As we discuss later in this section, such simulations are insufficient for understanding various biases.

Smith (1988) and Nerenberg & Essex (1990) considered boundary effect by calculating the correlation dimension for a hypercube or a hypersphere. These region geometries are not often encountered in earthquake statistics. De Luca *et al.* (1999, 2002) investigated boundary bias and location errors influence by simulation. Harte (1998, p. 602, see also Harte 2001, his section 11.3) discusses several effects that may cause bias in the correlation dimension estimates: 'boundary effect, lacunarity, rounding effect, and noise or location error', but again these effects are only analysed by simulation. We consider lacunarity or intermittency of spatial earthquake distribution as a natural consequence of its statistical self-similar pattern, for other biases analytic formulae are derived below to describe their influence.

These systematic effects are largely caused by geometrical factors. Many stochastic geometrical problems for point distribution in various figures are considered in http://mathworld.wolfram.com/topics/GeometricConstants.html (see also Wolfram 1999).

For some of these geometrical distributions we need to make assumptions which are not fully realistic. As a rule such assumptions are needed to obtain an analytic result. More general distributions can be obtained by simulations. However, theoretical expressions are still useful: first, they often are sufficient to understand the extent of an error or a systematic effect influence on results; secondly, the closed-form solutions are needed to check simulation programmes which may contain hidden flaws. The theoretical expressions below are usually represented in a form accessible to computation by standard software packages: FORTRAN, MATLAB, and MATHEMATICA. We list these expressions below, starting with those affecting the estimate for small distances between events (see also Kagan & Knopoff 1980; Kagan 1991a).

4.1 The number of earthquakes in a sample

Clearly the δ-value cannot be determined for distances less than the smallest distance ($r_{\min}$) between points. Strictly speaking, the fractal dimension of a point set is zero (Vere-Jones 1999), but in catalogue measurements $\delta = 0$ for $r \leq r_{\min}$ and should increase for greater distances. Nerenberg & Essex (1990) call this effect 'depopulation' and estimate the critical minimum distance as

$$r_{\min} = 2R \times (1/N)^{1/D}, \tag{9}$$

where N is the number of points in the cube of size $2R$, and D is the dimension of embedding Euclidean space.

Modern earthquake catalogues contain thousands and tens of thousands of events. Thus, unless we are interested in the distribution of only the strongest earthquakes, samples are well 'populated'. The distribution of events at small distances may be influenced by having too few earthquakes. As we will see, this distribution is more likely to be strongly biased by other effects.

4.2 Earthquake location error

The location error randomizes earthquake locations and, as a result, the correlation dimension estimate δ approaches D for distances less than or comparable to the average location uncertainty. In early catalogues, earthquakes and especially aftershocks, were often assigned a common location and depth. This decision reduces the δ-value (an example is shown in Fig. 14 below).

We assume that earthquake location errors are normally distributed and that errors for both points are independent of each other. The obtained earthquake locations for close events are most likely influenced by similar biases hence they are not statistically independent. However, in this work we measure the pairwise distances between earthquakes, thus only relative errors influence the result.

The distribution of distance r between the two epicentres or hypocentres whose actual separation is ρ obeys a 'non-central χ-distribution' (Fisher 1928; Kendall & Moran 1963, Chapter 5.19). Below we analyse this distribution for 3-D and 2-D earthquake spatial patterns (hypocentres and epicentres).

4.2.1 Earthquake location error: the 3-D case

Horizontal error is usually much smaller than vertical error. However, the general case of unequal errors cannot be analytically solved. If we assume for simplicity in a 3-D case that horizontal and vertical location errors are equal, the probability density of the 3-D non-central χ-distribution for hypocentres is

$$\phi(r|\rho) = \frac{r}{\rho\sqrt{2\pi}}\left[\exp -\frac{(r-\rho)^2}{2} - \exp -\frac{(r+\rho)^2}{2}\right]. \tag{10}$$

Both distances r and ρ are scaled by σ. If $\rho \to 0$, the distance distribution becomes the Maxwell law, with probability density function

$$\phi(r) = r^2\sqrt{\frac{2}{\pi}}\exp\left(-\frac{r^2}{2}\right). \tag{11}$$

The Maxwell law corresponds to the distribution of vector length in three dimensions, if the components of a vector are statistically independent and have a Gaussian distribution with the zero mean and the standard error σ. For large ρ distribution (10) becomes the Gaussian one (Fisher 1928, p. 664). The density is shown in Fig. 2.

If we assume that hypocentres are distributed over a fractal set with the dimension δ, then the number of events in a sphere of the radius R, centred on one of the points, that is, the number of pairs

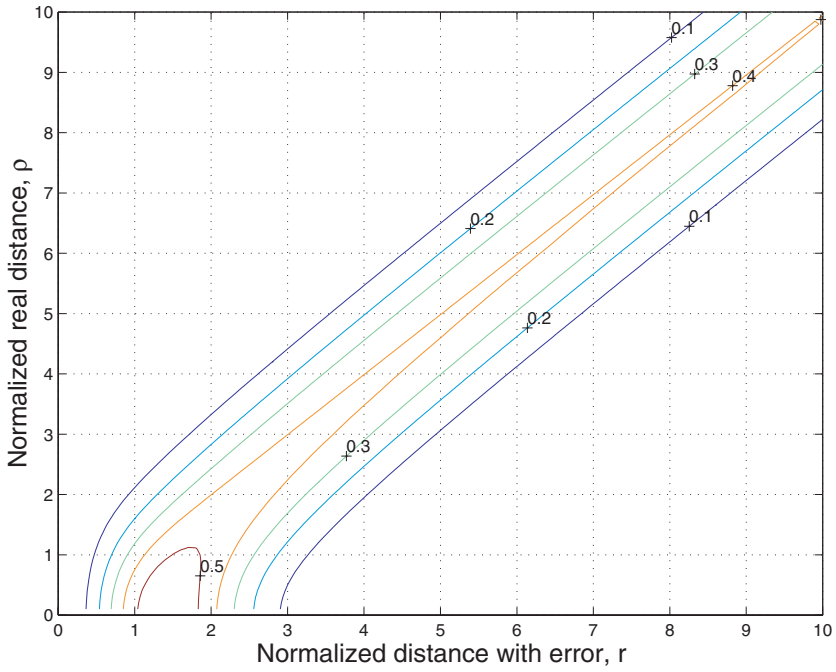

Figure 2. Density of non-central χ-distribution in 3-D.

in the 3-D space, $N_3(R)$, is

$$N_3(R) \propto \int_0^R dr \int_0^\infty \phi(r|\rho)\,\rho^{\delta-1}\,d\rho = \frac{2^{\delta/2}}{\sqrt{2\pi}}\,\Gamma\left(\frac{\delta}{2}\right)\int_0^R r^2\,\exp\left(-\frac{r^2}{2}\right)\,{}_1F_1\left(\frac{\delta}{2},\frac{3}{2},\frac{r^2}{2}\right)\,dr, \tag{12}$$

where Γ is a gamma function and ${}_1F_1$ is the Kummer confluent hypergeometric function (Abramowitz & Stegun 1972; Wolfram 1999).

For $\delta = 3$ the function ${}_1F_1\left(\frac{3}{2},\frac{3}{2},\frac{r^2}{2}\right)$ is $\exp\left(\frac{r^2}{2}\right)$, and for $\delta = 2$

$${}_1F_1\left(1,\frac{3}{2},\frac{r^2}{2}\right) = \frac{1}{r}\sqrt{\frac{\pi}{2}}\,\exp\left(\frac{r^2}{2}\right)\,\mathrm{erf}\left(\frac{r}{\sqrt{2}}\right), \tag{13}$$

where erf (R) is an error function. Then

$$N_3(R) \propto \int_0^R r\,\mathrm{erf}(r)\,dr = R\sqrt{\frac{2}{\pi}} \times \exp\left[-R^2/2\right] + \mathrm{erf}\left(\frac{R}{\sqrt{2}}\right)\left[R^2-1\right]. \tag{14}$$

The ratio $RN_3(R)/V_R$ can be estimated as

$$RN_3(R)/V_R = \frac{2}{R^2}\,N_3(R) = \sqrt{\frac{2}{\pi}} \times \frac{\exp\left[-R^2/2\right]}{R} + \mathrm{erf}\left(\frac{R}{\sqrt{2}}\right)\left[1-R^{-2}\right], \tag{15}$$

where V_R is a sphere volume. For other values of the dimension δ, the integrals (12) and eq. (20) below can be estimated numerically (Wolfram 1999).

Using (14) we estimate the correlation dimension for $\delta = 2$ in the presence of location errors as (4)

$$\hat{\delta} = \frac{\partial\left[\log N_3(R)\right]}{\partial\left(\log R\right)} = \frac{2\,R^2\,\mathrm{erf}\left(\frac{R}{\sqrt{2}}\right)}{N_3(R)}. \tag{16}$$

For large distances $\hat{\delta} \to 2$. For small values of the argument

$$\mathrm{erf}\left(\frac{R}{\sqrt{2}}\right) \approx R\sqrt{\frac{2}{\pi}} \times \exp\left[-R^2/2\right] \times \left[1+\frac{R^2}{3}\right], \tag{17}$$

(Abramowitz & Stegun 1972, eq. 7.1.6). Hence putting (17) in (16), we obtain that for small distances $\hat{\delta} \to 3$.

In Fig. 3, we show the dependence of $\hat{\delta}$ on the distance, both for simulation and computation according to (16). In a synthetic catalogue, we simulated 200 000 points on a 500 × 1000 km plane fault and then perturbed the location by adding the Gaussian errors. When calculating the $\hat{\delta}$-value, we compared the correlation function at distances separated by a factor $2^{1/4} = 1.189$.

4.2.2 Earthquake location error: the 2-D case

For the 2-D case of epicentres with location errors equal to σ, the non-central χ-distribution density is

$$\phi(r|\rho) = r\,\exp\left(-\frac{r^2+\rho^2}{2}\right)\,I_0\,(r\rho), \tag{18}$$

where I_0 is the modified Bessel function of 0th order. If $\rho \to 0$, the distance distribution becomes the Rayleigh law

$$\phi(r) = r\,\exp\left(-\frac{r^2}{2}\right), \tag{19}$$

which is a distribution of vector length in two dimensions (*cf.* eq. 11).

As in the 3-D case, we assume that epicentres are distributed over a set with the fractal dimension δ. Then the number of the events measured over the Earth's surface in a circle of the radius R, again centred on one of the points, that is, the number of pairs in the 2-D

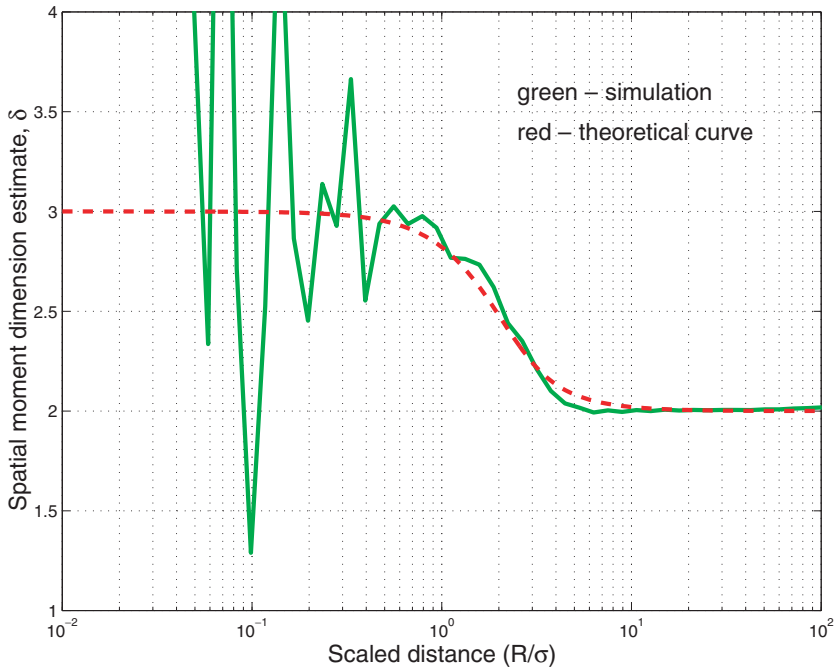

Figure 3. Dependence of the correlation dimension estimate $\hat{\delta}$ on distance scaled with the location error σ in 3-D. Solid line is simulation; dashed line shows $\hat{\delta}$ change according to eq (16).

space, $N_2(R)$, is

$$N_2(R) \propto \int_0^R dr \int_0^\infty \phi(r|\rho)\, \rho^{\delta-1}\, d\rho$$
$$= 2^{\delta/2-1}\, \Gamma\left(\frac{d}{2}\right) \int_0^R r\, \exp\left(-\frac{r^2}{2}\right)\, {}_1F_1\left(\frac{\delta}{2}, 1, \frac{r^2}{2}\right) dr, \quad (20)$$

see (12).

For $\delta = 1$

$${}_1F_1\left(\frac{1}{2}, 1, \frac{r^2}{2}\right) = \exp\left(\frac{r^2}{4}\right) I_0\left(\frac{r^4}{4}\right), \quad (21)$$

and for $\delta = 2$

$${}_1F_1\left(1, 1, \frac{r^2}{2}\right) = \exp\left(\frac{r^2}{2}\right). \quad (22)$$

In Fig. 4, we show the dependence of $\hat{\delta}$ on the scaled distance for hypocentres or epicentres displaced by the Gaussian errors with the standard deviation σ. We compute $\hat{\delta}$ according to (12) and (20). There is little difference between these curves as the underlying dimension of the point pattern changes. In the 2-D case, however, the curves are slightly displaced toward smaller values of the scaled distance.

4.3 Projection effect for epicentral scaling dimension

Assuming, for example, that hypocentres cover a fault-plane ($\delta = 2$), the epicentral correlation dimension may fluctuate from $\delta = 1$ to $\delta = 2$, depending on the dip angle of a fault. Thus, for distances comparable to the thickness of the seismogenic zone, the correlation dimension value should depend on the style of the earthquake deformation pattern. In the general case, projecting a 3-D distribution onto a 2-D plane is called 'grading' after Matheron (1971).

For illustrative purposes we have calculated the 2-D spatial moment, assuming both that the original seismicity is isotropic and the 3-D distance pair number function $N_3(R)$ is proportional to R^δ. Then a horizontal layer of seismicity of thickness W is projected on a horizontal plane:

$$G(R) = RN_2(R)/(\pi R^2)$$
$$\propto (2/R) \int_0^R r dr \int_0^W (W-h)(r^2+h^2)^{(\delta-3)/2}\, dh. \quad (23)$$

This integral is a complex expression involving hypergeometric functions.

For integer δ simpler expressions can be found. For $\delta = 1$

$$G(R) = W\left[2\, \arctan(A^{-1}) - \frac{1-A^2}{A}\, \log(B) + A\, \log(A)\right], \quad (24)$$

where $A = R/W$ and $B = \sqrt{1+A^2}$. For $\delta = 2$ we obtain the corrected eq. (3) in Kagan & Knopoff (1980)

$$G(R) = W^2\left[\frac{B-1}{A} + A\, \log\frac{B+1}{A} - \frac{2(B^3-A^3-1)}{3A}\right]. \quad (25)$$

And for $\delta = 3$

$$G(R) = W^3\, \frac{A}{2}, \quad (26)$$

In this case the ratio (or an estimate of the correlation dimension) does not depend on distance. This is to be expected since projecting uniformly 3-D distributed hypocentres on a surface produces a uniformly 2-D distributed pattern.

Using expressions (24–26) we can calculate an estimate of the correlation dimension for the grading problem:

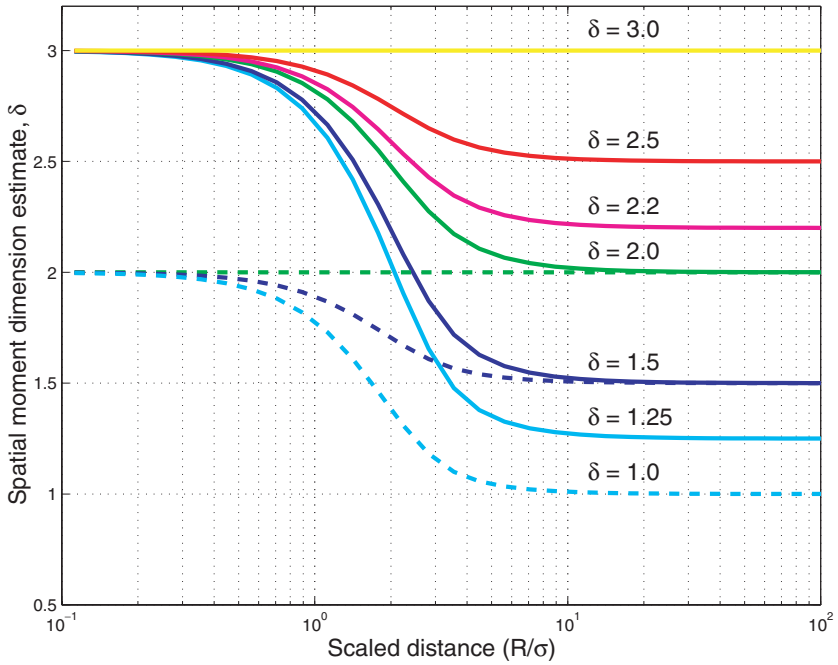

Figure 4. Dependence of the correlation dimension estimate $\hat{\delta}$ on distance scaled with the location error σ in 2-D and 3-D. Solid lines are for the 3-D distribution (hypocentres); dashed lines are for the 2-D distribution (epicentres). The initial fractal point dimension indicated as $\delta = 3$, etc.

$$\hat{\delta} = 1 + \frac{\partial (\log G)}{\partial (\log R)}. \tag{27}$$

In particular for $d = 1$

$$\hat{\delta} = \frac{2\,A\,\left[\arctan\left(\frac{1}{A}\right) - A\,\log\left(\frac{B}{A}\right)\right]}{2\,A\,\arctan\left(\frac{1}{A}\right) - A^2\log\left(\frac{B}{A}\right) + \log(B)}, \tag{28}$$

for $d = 2$

$$\hat{\delta} = A^2\frac{2\log\left(\frac{1+B}{A}\right) + \frac{6A-4B-3}{3} + \frac{1+B-2A^2B+A^2}{3B(1+B)}}{A^2\,\log\left(\frac{1+B}{A}\right) + \frac{2A^3-1+B(1-2A^2)}{3}}, \tag{29}$$

and for $d = 3$

$$\hat{\delta} \equiv 2. \tag{30}$$

In Fig. 5, we show the dependence of $\hat{\delta}$ on the distance scaled with the width of a seismogenic layer (W). Three distributions of the points are assumed in the layer: with $\delta = 1$; $\delta = 2$; and $\delta = 3$ (i.e. uniform Poisson distribution). The correlation dimension is determined for the projection of the points on a horizontal plane (equivalent to the epicentres). We display both theoretical values of the dimension (eqs 28–30, respectively) and the simulated values again evaluated at distances separated by a factor $2^{1/4}$.

The curves show the expected behaviour: for small scaled distances $\hat{\delta} \rightarrow \delta - 1$ as the result of projection (Mandelbrot 1983), but for large distances $\hat{\delta} \rightarrow \delta - 2$. For the Poisson point distribution in a layer, the point pattern projected on a surface has a uniform $\hat{\delta} = 2$.

4.4 Boundary effects

For practical measurements when the size (diameter) of the set explored exceeds the distance r, the correlation function stops increasing. Nerenberg & Essex (1990) call this effect 'saturation' and estimate the critical minimum distance as

$$r_s = R/(D + 1). \tag{31}$$

As in (9) $2R$ is the side of a cube and D is the embedding dimension. If $r > r_s$ in the correlation function $C(r)$, the function is saturated: its value does not represent the scaling effect of a point pattern.

For local and regional earthquake catalogues, the spatial boundaries delineate the area of sufficient coverage. For distances comparable to the area size, the δ-value estimate is biased depending on how the fault system pattern relates to the area polygon. If, for example, a narrow rectangular box were oriented along the direction of the major faults or perpendicular to them, this bias would significantly differ.

Below we consider a few simple cases where $\hat{\delta}$ can be analytically derived. The distribution of the distances in more complicated polygons and other figures can be obtained by a simulation.

4.4.1 Boundary effects: a 2-D case

The simplest 2-D figure is a disc. For points in a disc of diameter d, the distribution density for normalized distance $y = r/d$ between two random points inside is (Hammersley 1950)

$$\phi(y) = \frac{16\,y}{\pi\,d}\left[\arccos(y) - y\sqrt{1-y^2}\,\right]. \tag{32}$$

The surface area for the box in Fig. 1 is $S \approx 233\,300$ km^2. Approximating it by a circle, we obtain its radius as 272.5 km. When calculating temporal correlation functions, 10 per cent of the time interval is usually considered the upper limit for reliable estimation. In southern California this would suggest that for distances over 25–50 km, the $\hat{\delta}$ values are more questionable.

Garwood (1947) and Ghosh (1951) propose formulae to calculate the distribution density for distances r between random point pairs

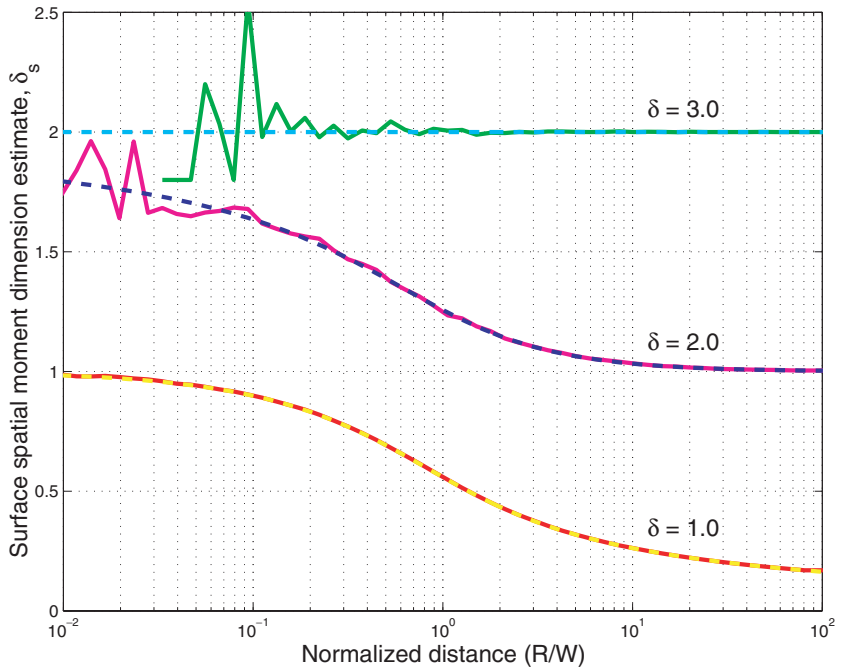

Figure 5. Dependence of the correlation dimension estimate $\hat{\delta}$ on scaled distance for epicentre distribution (grading effect). Three distributions in a layer of thickness W are simulated in 3-D: $\delta = 3$ or uniform Poisson distribution (upper two curves), with $\delta = 2$ (middle two curves), and with $\delta = 1$ (lower two curves). Dashed lines are theoretical curves (eqs 28–30); solid lines are simulation results.

in a rectangular box $a \times b$ for $a > b$:

$$\phi_1(r) = \frac{2r}{a^2\,b^2}\left[a\,b\,\pi - 2\,r\,(a+b) + r^2\right] \quad \text{for } r \le b, \tag{33}$$

$$\phi_2(r) = \frac{4r}{a^2\,b^2}\left[a\sqrt{r^2-b^2} - \frac{b^2}{2} - a\,r + a\,b\,\arcsin\left(\frac{b}{r}\right)\right] \quad \text{for } b < r \le a, \tag{34}$$

and

$$\phi_3(r) = \frac{4r}{a^2\,b^2}\left[a\sqrt{r^2-b^2} + b\sqrt{r^2-a^2} - \frac{1}{2}\left(a^2+b^2+r^2\right) - a\,b\,\arccos\left(\frac{a}{r}\right) + a\,b\,\arcsin\left(\frac{b}{r}\right)\right], \tag{35}$$

for $a < r \le \sqrt{a^2+b^2}$.

4.4.2 Boundary effects: 3-D case

Here, we discuss a distribution of distances in a horizontal layer of width W in a 3-D space. This would correspond to the average number of hypocentre pairs within a distance R of an arbitrary point in a layer of uniformly distributed seismicity. Three cases need to be considered: a sphere of radius R not touching any layer boundary, a sphere intersecting only one boundary, and another intersecting both boundaries.

For various distance ranges, we obtain three expressions. For $R < W/2$

$$N_3(R) = \frac{4\pi\,(W-2R)\,R^3}{3W} + \frac{2\pi}{3W}\int_0^R (2\,R-h)\,(R+h)^2 dh = \frac{\pi R^3}{6W}\,(8\,W - 3R). \tag{36}$$

For $W > R > W/2$ as in (36)

$$N_3(R) = \frac{2\pi}{3}\int_0^{W-R}(2\,R-z)\,(R+z)^2\,dz + \frac{2\pi}{3}\int_{W/2}^{R}\Big[4\,R^3 - (R-z)^2\,(2\,R+z) - (W+2\,R-z)\,(R-W+z)^2\Big]dz = \frac{\pi\,R^3}{6W}\,(8\,W - 3\,R)\,. \tag{37}$$

For $R > W$

$$N_3(R) = \frac{\pi}{3W}\int_0^{W}\Big[4\,R^3 - (R-h)^2\,(2\,R-h) - (W+2\,R-h)\,(R-W+h)^2\Big]dh = \pi W^2\left(R^2 - \frac{W^2}{6}\right). \tag{38}$$

For $R < W$ the estimate of correlation dimension is

$$\hat{\delta} = \frac{12\,(2\,W - R)}{8\,W - 3\,R} = \frac{12\,(2-\rho)}{8 - 3\,\rho}, \tag{39}$$

where $\rho = R/W$. For $R > W$ it is

$$\hat{\delta} = \frac{2\,R^2}{R^2 - W^2/6} = \frac{2\,\rho^2}{\rho^2 - 1/6}. \tag{40}$$

As expected, for $\rho \to 0$ the hypocentral correlation dimension estimate $\hat{\delta} \to 3$ and for $\rho \to \infty$ the dimension $\hat{\delta} \to 2$.

4.5 Inhomogeneity of earthquake depth distribution

Inhomogeneity of earthquake depth distribution influences the hypocentral fractal dimension. If this distribution were in fact

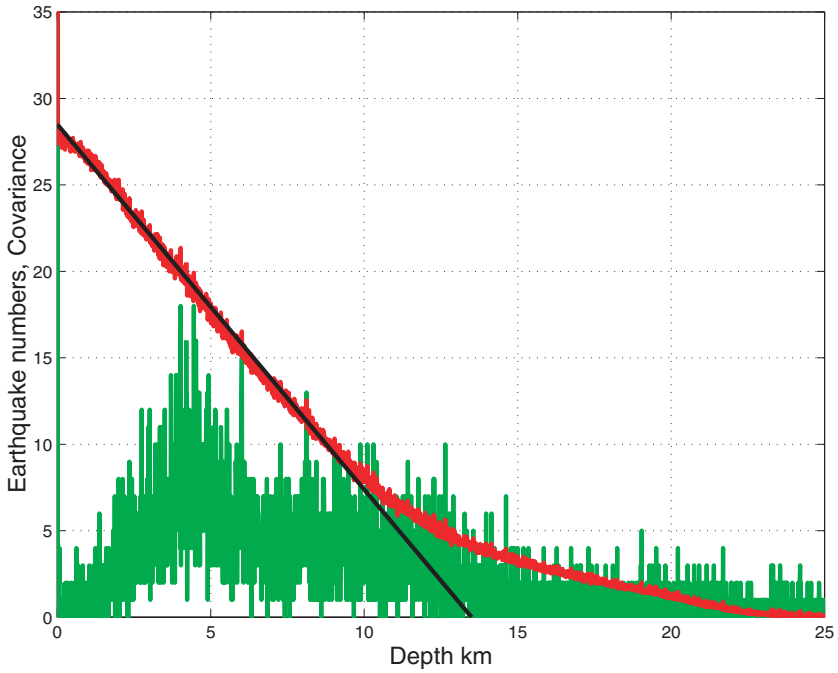

Figure 6. Depth dependence histogram (green lines) for the Hauksson & Shearer (2005) catalogue ($M_c = 3$). Same events as in the box in Fig. 1. Depth correlation function (red line) and its approximation by linear function (black line), corresponding to a layer of thickness 13.5 km with uniform distribution of seismicity with depth.

uniform over depth, the dimension estimate would approach the real δ-value for distances smaller than the thickness of the seismogenic zone (see eqs 39–40). Otherwise, the apparent dimension value is effectively a convolution of the scale-invariant distribution with a non-uniform depth distribution.

We correct the hypocentral moment for the non-uniformity of the earthquake depth distributions:

$$G(R) = RN_2(R)/(\pi R^2) \propto (2/R)\int_0^R r\,dr \int_0^r K(z)\,(r^2+z^2)^{(\delta-3)/2}\,dz. \quad (41)$$

Here, $K(z)$ is the depth covariance function

$$K(z) = (\Delta h)^{-2}\int_{h_1}^{h_2} N(h,\ h+\Delta h)\,N(h+z,\ h+z+\Delta h)\,dh, \quad (42)$$

where $N(h, h+\Delta h)$ is the number of hypocentres in Δh depth interval, h_1 and h_2 are depth limits: for example, for global shallow seismicity, $h_1 = 0$ and $h_2 = 70$ km. The integrals in eqs (41) and (42) can be evaluated numerically for a known distribution $N(h)$. The similarity between (23) and (41) is not accidental, since $C\,(W-h)$ is a correlation function (C is a normalizing coefficient) for the number of hypocentres in a layer W, if hypocentres are distributed uniformly over depth.

In Fig. 6, we display the distribution of the hypocentre numbers for the Hauksson & Shearer (2005) catalogue as well as the correlation function (42). We used the magnitude threshold $M_c = 3$, since the depth accuracy of these earthquakes should be higher. Most of the correlation function can be approximated by a linear function $C\,(W-h)$ with $W = 13.5$ km.

For $d = 3$, that is, the Poisson 3-D distribution of hypocentres with depth density $N(h, h+\Delta h)$, the pair number distribution is

$$N_3(R) = \frac{4\pi}{S}\int_0^R r\,dr \int_0^r K(z)\,dz, \quad (43)$$

where S is the surface area spanned by a catalogue. Putting $K(z) = C\,(W-z)$ in (43), corresponding to a covariance function for a layer with uniform seismicity, we recover (36). For distances longer than $W/2$, the covariance function can be padded by zeros. Thus, we do not need to calculate more complicated formulae (37) and (38).

In Fig. 7, we show two curves to account for depth inhomogeneity. One is based on the depth correlation function (43); another uses eqs (36)–(38) to calculate pair numbers in a layer with width 13.5 km. As Fig. 6 demonstrates, the correlation function of the hypocentral depth distribution is well approximated by a linear fit. Hence, both curves in Fig. 7 almost coincide.

In this figure as well as in several subsequent plots (Figs 8, 9 and 11) we scale the number of earthquake pairs N_D by dividing the number by distance R or by its square R^2. This is done to reduce the size of the plots and simplify them.

It may seem from Fig. 7 that we can correct for depth inhomogeneity without eqs (41)–(43). However, the depth distribution in other earthquake catalogues may be more difficult to approximate by a uniformly distributed point pattern. For example, in global catalogues of shallow earthquakes, many events are assigned the depth of 10 and 33 km, making the covariance function highly 'spiky'.

4.6 Earthquake pattern depth influence

Earthquake depth influences the degree of seismic coupling: it determines which part of the tectonic deformation is released by earthquakes. Apparently, for shallow subduction and continental earthquakes, the coupling coefficient is close to 1.0 (McCaffrey 1997; Bird & Kagan 2004). For deeper earthquakes, most of the tectonic motion is accommodated by plastic deformation (Kagan 1999). In global catalogues deep earthquake locations are more clustered than

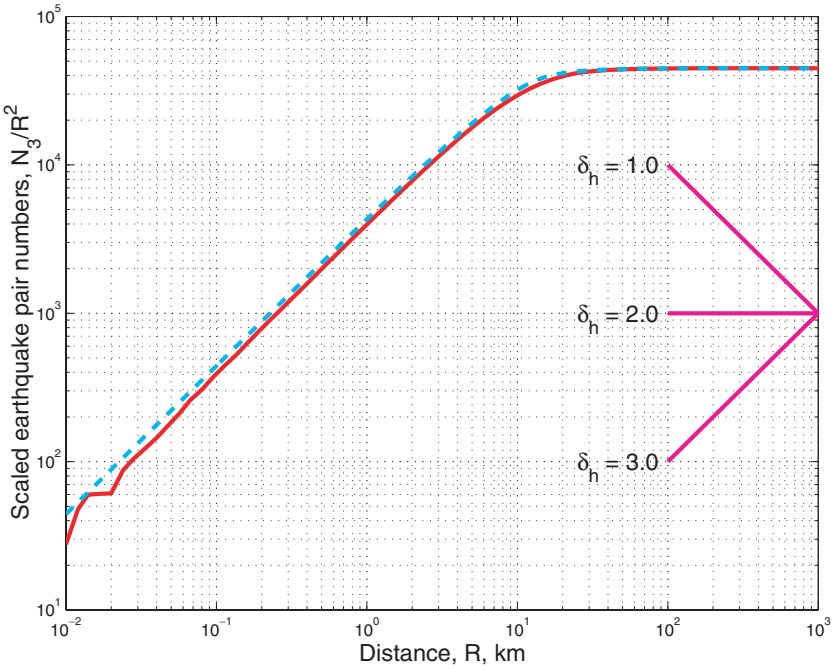

Figure 7. The expected number of event pairs in the southern California catalogue. The theoretical curve (dashed line) is calculated for a layer with width $W = 13.5$ km having uniform seismicity distribution (39, 40). The solid line is the estimate for the Hauksson & Shearer (2005) catalogue ($M_c = 3$), corrected (43) by using the correlation function shown in Fig. 6. We normalize (divide) the earthquake pair number by R^2 so that the horizontal line would correspond to $\delta = 2$.

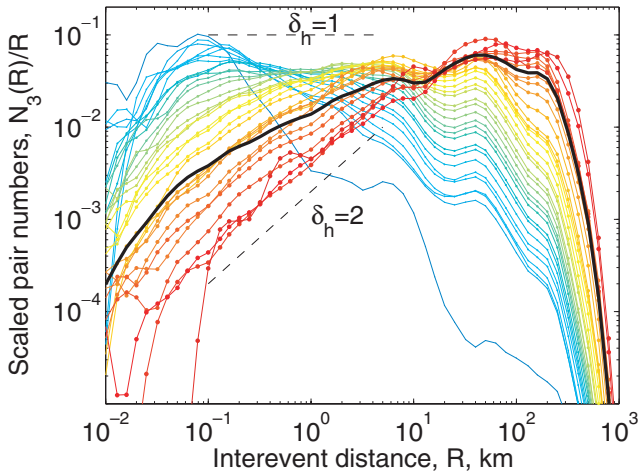

Figure 8. Distribution of distances between hypocentres $N_3(R, t)$ for the Hauksson & Shearer (2005) catalogue, using only earthquake pairs with interevent times in the range $[t, 1.25t]$. Time interval t increases between 1.4 min (blue curve) to 2500 days (red curve). We normalize (divide) the earthquake pair number by R so that the horizontal line would correspond to $\delta = 1$. The black line is the function $N_3(R)$ measured for all earthquake pairs; it has a fractal dimension $\hat{\delta} \approx 1.5$ for $0.1 \leq R \leq 5$ km.

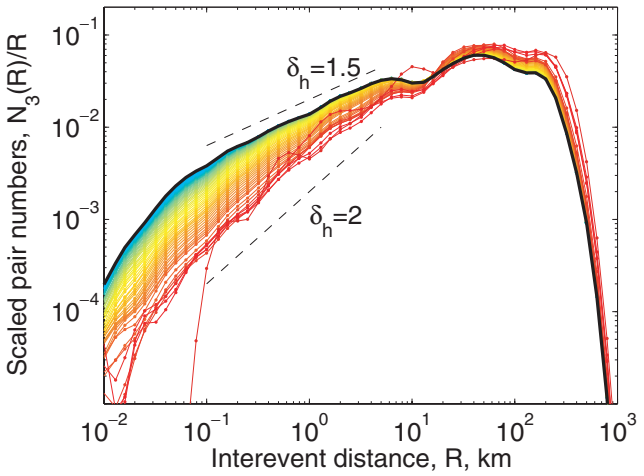

Figure 9. This diagram is similar to Fig. 8 but for pairs with interevent times larger than t.

those of shallow seismicity, and the δ-value decreases (see Kagan & Knopoff 1980; Kagan 1991a, and Fig. 18 below).

Wyss *et al.* (2004) attempted to determine the correlation dimension for shallow earthquakes in a creeping section of the San Andreas fault near Parkfield. They found that the spatial earthquake distribution shows no scale-invariant distance range. Hence the $\hat{\delta}$-value is not well defined for this region.

4.7 Temporal influence

For small time intervals, earthquakes are more clustered and their correlation dimensions are smaller (Kagan 1991a; Helmstetter *et al.* 2005). This is perhaps the most important issue influencing the δ-value estimate. The previous items in this section influence the estimate for a limited distance range only and hence can be recognized and compensated, or alternatively these distance ranges can be ignored in the correlation dimension calculation. However, time dependence extends over all distance intervals and cannot be that easily corrected.

We have estimated the distribution of distances between hypocentres $N_3(R)$, using the Hauksson & Shearer (2005) catalogue (Section 3). We have selected only $M \geq 2$ earthquakes relocated with an

accuracy of ϵ_h (horizontal) and ϵ_z (vertical) smaller than 0.1 km. In the catalogue, there are 82442 $m \geq 2$ earthquakes in the time period [1984, 2002], out of which 33676 (41 per cent) are relocated with $\epsilon_h < 0.1$ km and $\epsilon_z < 0.1$ km (see also Helmstetter *et al.* 2005, their fig. 5).

The distance number function of $N_3(R)$ between the hypocentres is close to a power-law $N_3(R) \propto R^{\delta}$ in the range $0.1 \leq R \leq 5$ km. The correlation fractal dimension (measured by least-square linear regression of $\log(R)$ and $\log[N_3(R)]$ for $0.1 \leq R \leq 5$ km) is $\hat{\delta} \approx 1.5$ (black lines in Figs 8 and 9). The faster decay for $R < 0.1$ km is due to location errors (Section 4.2.1), and the roll-off for distances $R > 5$ km is due to the finite thickness of the seismogenic crust (Section 4.4.2). For larger distances ($R > 50$ km), the $\hat{\delta}$ decrease is caused by catalogue boundaries (Section 4.4.1).

To estimate the time dependence of the spatial distribution of interevent distances, we have measured the distribution $N_3(R, t)$, using only earthquake pairs with an interevent time τ in the range $[t, t + dt]$ (Fig. 8). We have also computed the distribution

$$N_3(R, \tau \geq t) = \int_t^T N_3(R, t')\, dt', \tag{44}$$

cumulated over all times larger than t (only using events with interevent times larger than t up to $T = 2500$ days, see Fig. 9).

As the minimum interevent time increases, the fraction of small distances will decrease. For interevent times larger than 1000 days, the fractal dimension of the cumulative distribution $N_3(R, \tau \geq t)$ increases with t from the value measured for the whole catalogue ($\hat{\delta} \approx 1.5$) to a maximum value close to 2. For $N_3(R, t)$, $\hat{\delta}$ increases between $\hat{\delta} \approx 0$ at times $t = 5$ min up to $\hat{\delta} \to 2$ for $t = 2500$ days (Fig. 10). This maximum interevent time of 2500 days is long enough so that earthquake interactions are relatively small compared to the tectonic loading. Only an insignificant fraction of earthquake pairs are triggering-triggered events. This value $\hat{\delta} = 2$, measured for $t = 2500$ days, can thus be interpreted as approaching the fractal dimension of the active fault network.

However, Fig. 10 clarifies that $\hat{\delta} \to 2$ is not an asymptotic limit for the correlation dimension. The $\hat{\delta}$-value continues to increase. The time interval for the Hauksson & Shearer (2005) catalogue (1984–2002) is too short for the $\hat{\delta}$ to reach the final value. As we mentioned earlier, in a local catalogue the seismicity pattern for larger time intervals is strongly influenced by a few strong earthquakes and their aftershocks (Section 1).

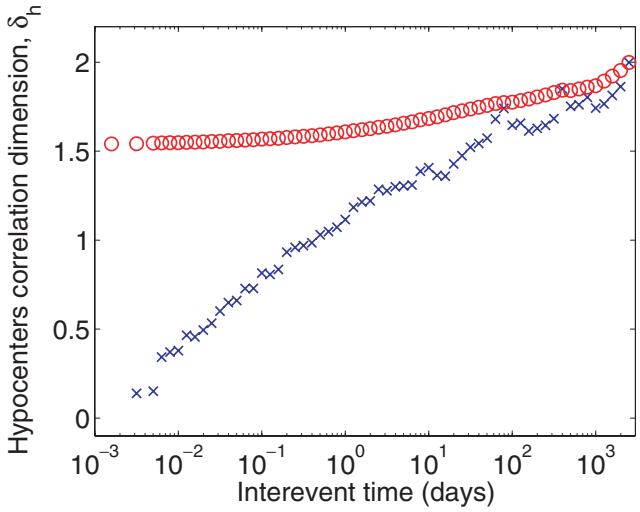

Figure 10. Fractal dimension of Fig. 8 curves (crosses) and of Fig. 9 curves (circles) as a function of time interval t. Distance interval is $0.1 \leq R \leq 5$ km.

The results for global catalogues yield a better measure of the asymptotic $\hat{\delta}$-value. In such cases the range of the correlation dimension change is also large. For shallow earthquakes, $\hat{\delta}$ varies from 1.2 to 2.1 (table 2 in Kagan 1991a) for time intervals of 1.0–8575 days. Furthermore, whereas the results shown in Figs 8–10 may be explained by a strong spatial concentration of aftershocks for several large Californian earthquakes, figs 2 and 3 in Kagan (1991a) demonstrate that this temporal effect is present in the PDE global catalogue, both the original and declustered one.

The great variability of the $\hat{\delta}$-value with time intervals is important. Whereas previous items (in Sections 4.1–4.6) are discussed in spatial analyses of earthquake patterns (see references in Section 1), little is done to address the temporal aspect. Most likely, the full statistical analysis of this problem would require taking into account tectonic and seismic deformation rate in various types of plate boundaries (Bird & Kagan 2004).

The strong dependence of the correlation dimension on time contradicts the widely used Aki's (1981) hypothesis of connection between the b-value of the Gutenberg–Richter law (Bird & Kagan 2004) and the δ-value. Indeed, the b-value is largely independent of time (Kagan 2004). In some publications (Wyss *et al.* 2004, and references therein) it is suggested that the b-value can vary by a factor 1.5–2, but this change is not proposed for different time intervals but rather for various spatial and tectonic regions. However, even such b-value fluctuations cannot be matched by a strong variation of the δ-value (see above). Hence, the b-value cannot define the temporally dependent earthquake fractal spatial dimension (see also discussion by Kagan 1991b, p. 132).

4.8 Randomness

Finally, we mention the randomness of earthquake occurrence. Even when all other effects are taken into account, earthquakes occur randomly in time and space.

Moreover, because of earthquake clustering, especially the short-term which expresses itself in foreshock–mainshock–aftershock sequences, the effects of randomness are stronger than for a Poisson process (Vere-Jones 1999). Local catalogues often contain large aftershock sequences which make up a significant part of the total. Therefore, though such catalogues list many thousands of earthquakes, the effective size of a sample may amount to considerably fewer events. Consequently, random fluctuations can be quite strong. An example of such a gross fluctuation is shown in Fig. 12 below.

5 CORRELATION DIMENSION FOR EARTHQUAKE CATALOGUES

5.1 Corrections for errors and biases

In this section, we use the results of Section 4 to take into account and sometimes correct the observed distance distributions.

5.1.1 Example

Fig. 11 displays the spatial hypocentral and epicentral moment curves for the Hauksson & Shearer (2005) catalogue (Section 3). The distance scale is increased by a factor of $2^{1/4}$, starting with $R = 0.01$ km. In Fig. 12, we show the estimate of the correlation dimension $\hat{\delta}$, calculated by a formula equivalent to (16). At the distances

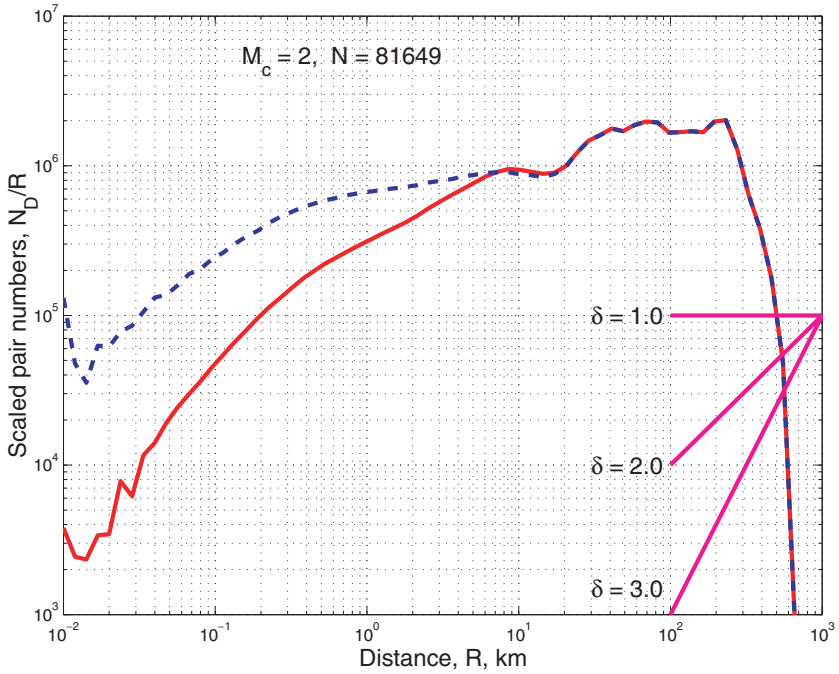

Figure 11. Hypocentral and epicentral spatial moment curves for the southern California waveform cross-correlation catalogue 1984–2002 (Hauksson & Shearer 2005). Same events as in the box in Fig. 1. The magnitude threshold is $M_L \geq 2.0$, the total number of earthquakes $N = 81649$. The solid curve is for the hypocentral moment and the dashed for the epicentral.

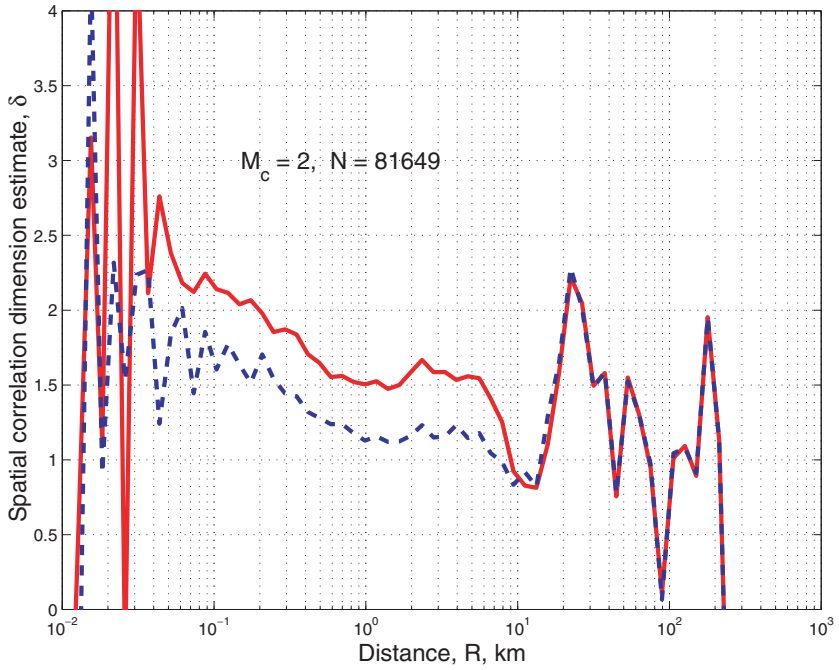

Figure 12. Correlation dimension estimate ($\hat{\delta}$) for the 1984–2002 Hauksson & Shearer (2005) catalogue (Fig. 11). The solid curve is for the hypocentral moment and the dashed for the epicentral. The correlation dimension values are calculated as the distance scale is increased by a factor of $2^{1/4}$, starting with $R = 0.01$ km.

$R < 0.1$ km, random scatter (Section 4.8) dominates the pattern, although the relatively high values of average $\hat{\delta}$ can be clearly attributed to location errors (Section 4.2). The location error effects would be strong for distances $0.01 < R < 1.0$ km (in this subcatalogue we did not delete the earthquakes with low location accuracy, as was done in Figs 8–10). For distances approaching 10–15 km, the finite thickness of the seismogenic zone strongly influences the hypocentral dimension (Section 4.4.2 and Fig. 7).

The epicentral $\hat{\delta}$-value is close to 2.0 for small distances. This is likely due to the location errors (Fig. 4) and projection (Fig. 5), although the latter effects should be relatively small since most faults in southern California are almost vertical.

The difference between the hypocentral and epicentral correlation dimensions at larger distances (1–10 km) is due mostly to projection effects (Section 4.3). From Fig. 5 we see that for isotropic point distribution with $\delta = 2$, the epicentral correlation dimension should decay from $\hat{\delta} = 1.5$ to $\hat{\delta} = 1.0$ in the scaled distance range $R/W = [0.1 - 10.0]$. If earthquakes were distributed on vertical faults, the difference between the two dimensions would be exactly 1.0 ($\hat{\delta}_h = 2.0, \hat{\delta}_s = 1.0$) and independent of distance. (Here δ_h is the correlation dimension for the hypocentral moment and δ_s is the dimension for the epicentral one.) For the horizontally dipping faults both dimensions would be the same. In the California catalogues the spatial earthquake distribution mixes the above-mentioned patterns with a prevalence of vertical strike-slip faults. Thus, in Fig. 12 the difference between the dimensions is on the order of 0.5, and both dimensions decay with distance.

For distances exceeding the effective thickness of the seismogenic layer ($W = 13.5$ km), the epicentral and hypocentral moments practically coincide (see Section 4.5). Random fluctuations associated with aftershock clusters of a few major earthquakes again predominate at larger distances. Finally, for distances approaching the size of the box in Fig. 1 (hundreds km), the spatial boundary effects (see Section 4.4.1) strongly decrease correlation dimension.

5.1.2 Corrections and normalizations

We consider how the spatial moments can be corrected for the effects discussed in Section 4. Location errors are obvious targets for such a correction. Unfortunately, although these errors are studied extensively and many catalogues contain internal estimates of such uncertainties based on the discrepancy in fitting the arrival times, there are many difficulties in applying our expressions (Section 4.2). The internal errors are only part of the total location uncertainties, as we see in analysing the earthquake catalogue accuracy (Kagan 2003). Real location errors, including systematic ones, are often significantly higher.

Location errors vary over the time span and territory of catalogues. This is especially true for local catalogues. Catalogues based on the waveform cross-correlation have a high relative location accuracy for earthquake clusters where such correlation is feasible. However, for different clusters, associated relative error may be significantly higher.

To save effort and the paper size, we refrained in this work from correcting location errors and projection effects. Such procedures can be implemented in future studies of earthquake spatial distributions.

In Fig. 13, we show the epicentral and hypocentral curves for the Hauksson & Shearer (2005) catalogue (Section 3), normalized by dividing $N_2(R)$ and $N_3(R)$ numbers by the appropriate pair numbers in a Poisson process. For the 2-D pattern, Poissonian epicentres are randomly distributed inside the box shown in Fig. 1. For distances comparable to the box size, we estimate the distribution of pair numbers, $N_2^p(R)$, using simulated catalogue (cyan curve in Fig. 13). To avoid random fluctuations, when distances are small, we calculate

$$N_2^p(R) = \frac{N(N-1)}{2} \times \frac{\pi R^2}{S}, \tag{45}$$

where S is the area of the box, and N is the number of points in a catalogue. We combine both simulated and theoretical curves at $R = 3$ km.

The normalized epicentral curve in Fig. 13 is the ratio

$$N_2^n(R) = \frac{R}{R_{\max}} \times \frac{N_2(R)}{N_2^p(R)}, \tag{46}$$

where $R_{\max} = 734.5$ km is the maximum distance in the box, and multiplication by $R/R_{\max}$ is done to make the curve approximately

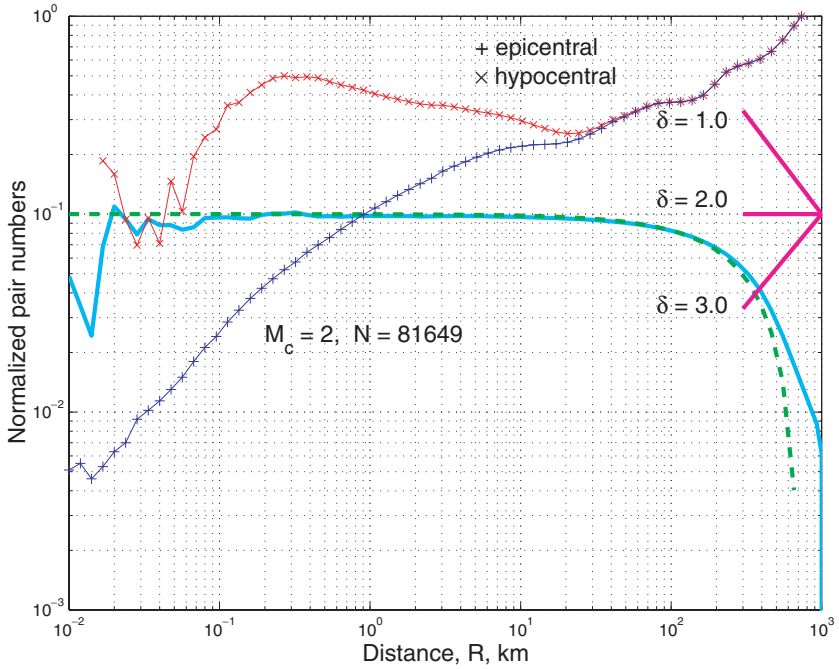

Figure 13. Hypocentral and epicentral spatial moment curves for the southern California waveform cross-correlation catalogue 1984–2002, $M_L \geq 2.0$ (Hauksson & Shearer 2005). Same events as in the box in Fig. 1. The upper curve is for the hypocentral moment and the lower for the epicentral. Here we also plot two curves, demonstrating the boundary effects due to the limited spatial size of the catalogue (see Section 4.4.1). The cyan solid curve is obtained by simulation for the box in Fig. 1. The green dashed line is calculated for a circle of radius 734.5 km (the maximum distance in the box). Magenta lines at the right show a slope of the curves corresponding to the integer values of the correlation dimension for the epicentral moment $\delta_s = \delta_h - 1$.

horizontal for $\delta_s = 1$ and to normalize the value of the moment at the maximum distance.

A similar normalization is carried out for the hypocentral moment. For small distances, we compute $N_3^p(R)$ using (43). We multiply the ratio of the observational curve to the Poisson one by $R/R_{\max}$, as in (46). Since the Poisson pattern has the dimension 3 here, the horizontal curve means that the hypocentral distribution has $\delta_h = 2$. The curves below the horizontal line have $\delta_h \geq 2.0$ (the fractal dimension is equal to the tangent of the slope angle of the curve plus 2.0). In one plot we combine two types of curves, epicentral and hypocentral, to show their difference.

The described normalizations rectify for the boundary effects. In the 2-D case, the correction relates to the box boundaries; in the 3-D case the bias due to the inhomogeneity of the depth distribution is also corrected. However, as we explained in Section 4, these corrections make certain assumptions about the actual spatial distribution of earthquakes. It is not clear whether these assumptions are fully valid. However, when comparing Fig. 11 with Fig. 13 where the corrections are applied, we see that such corrections increase the range of the scale-invariant behaviour of the moments. The normalization, applied in Fig. 13, is used in all subsequent diagrams (Figs 14–18). Similarly, in these diagrams the corrections extend the power-law moment range.

5.2 California catalogues

Figs 14 and 15 display the spatial moment curves for the CalTech (CIT) catalogue (Hileman *et al.* 1973) in two periods: 1932–2001 and 1975–2001. The curves' behaviour for small distances demonstrates the influence of location errors and catalogue compiling procedures. In the first plot for distances smaller than 3 km, the fractal correlation dimension is less than 1.0. The most likely reason for this is that during the first years of the CalTech catalogue, the aftershocks were often assigned the same location as the main shocks (see Section 4.2). This choice makes the dimension of an aftershock sequence equal to zero. Because many sequences are present in this catalogue, the combined dimension is small, while not being a zero.

In the second plot (Fig. 15), only recent earthquakes have been processed. The hypocentral correlation dimension for small distances (0–5 km) is close to 3.0. This value results from location errors which randomize the position of hypocentres and from projection effects (see Section 4.2).

Both curves' behaviour at large distances (more than 100–200 km) is controlled by box boundary effects (see Section 4.4). In these plots we did not account for such effects as we had in Fig. 13. The scale-invariant part of the curves is in a distance range of 2–200 km, where the correlation dimension is slightly over 2.0. As explained in Section 4.8, the curves' fluctuations are probably caused by large aftershock sequences of the 1992 Landers, 1994 Northridge, and 1999 Hector Mine earthquakes.

Fig. 16 displays similar spatial distribution for the catalogue of relocated earthquakes (Richards-Dinger & Shearer 2000). The higher location accuracy of these events is seen in the extension toward smaller distances of the scale-invariant region. Whereas the time span in both diagrams (Figs 15 and 16) is approximately the same, the hypocentral moment in the latter plot extends as a power law from about 0.5 km up to 200 km. The difference between the epicentral and hypocentral curves is larger for the Fig. 16 diagram. This is due to a higher accuracy of hypocentral solutions. If the vertical errors were comparable to the thickness of the seismogenic zone, the curves would be almost identical for distances comparable to the thickness (Kagan & Knopoff 1980).

Fig. 13 displays similar spatial distribution curves for the waveform cross-correlation catalogue by Hauksson & Shearer (2005). The clusters of earthquakes in the catalogues have been cross-correlated to obtain relative accuracy on the order of tens of metres. Two distance intervals can be seen in the curves: 0.2–20 km and 20–200 km. Apparently the catalogue has two earthquake populations:

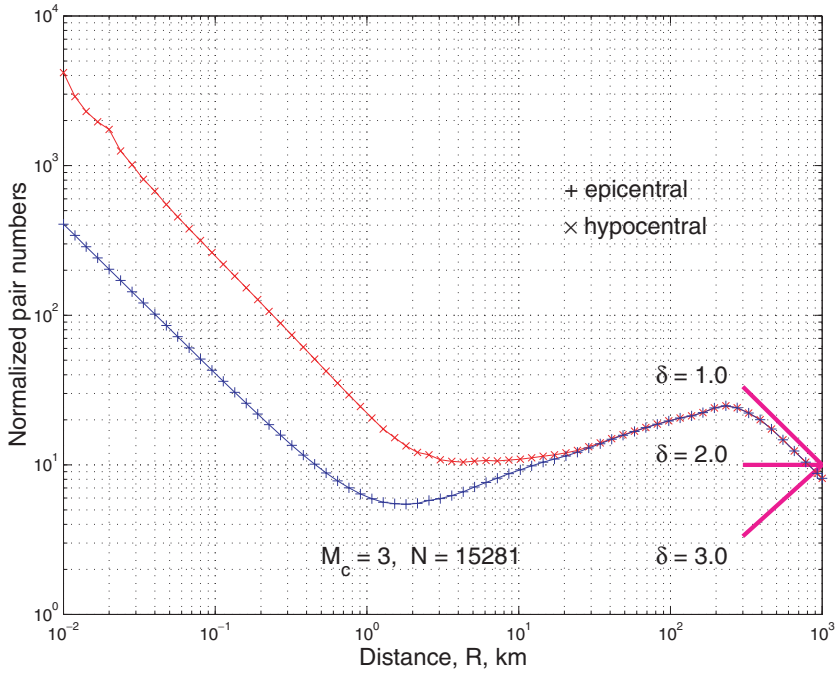

Figure 14. Hypocentral and epicentral spatial moment curves for the southern California (CalTech) catalogue 1932–2001. Same box as in Fig. 1. The upper curve is for the hypocentral moment and the lower for the epicentral.

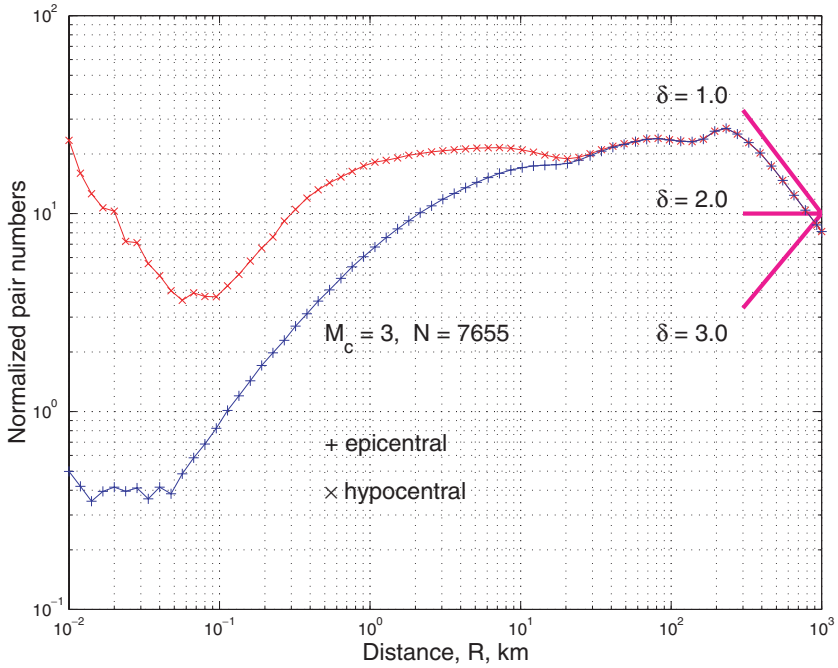

Figure 15. Hypocentral and epicentral spatial moment curves for the southern California (CalTech) catalogue 1975–2001 ($M_L \geq 3.0$). Same box as in Fig. 1. The upper curve is for the hypocentral moment and the lower for the epicentral.

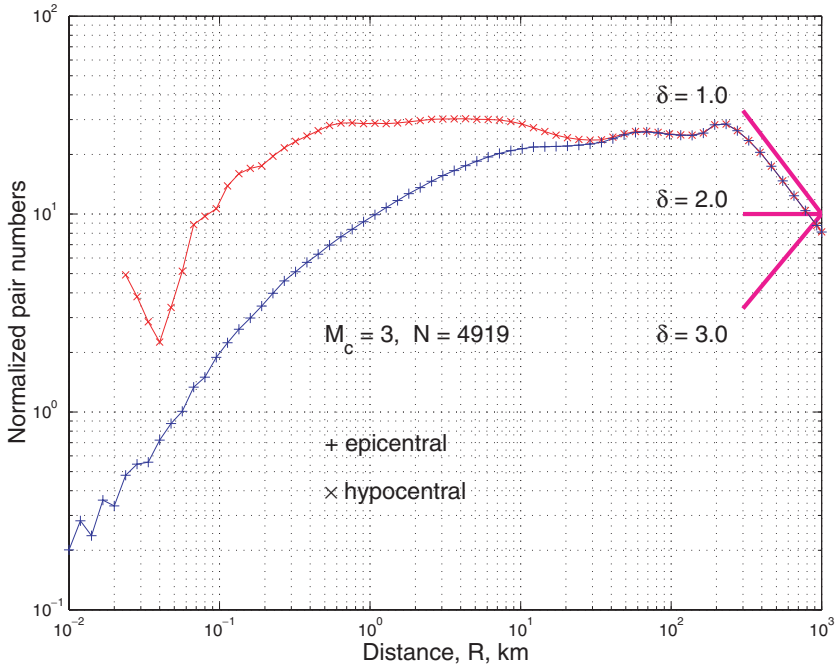

Figure 16. Hypocentral and epicentral spatial moment curves for the southern California relocated earthquake catalogue 1975–1997 (Richards-Dinger & Shearer 2000). Same box as in Fig. 1. Magnitude threshold is $M_L \geq 3.0$. The upper curve is for the hypocentral moment and the lower for the epicentral.

one corresponding to the events in the cross-correlation clusters and the other to the intercluster distances. The small distance part ($R = 0.01$–0.2 km) of the hypocentral curve indicates that the earthquake spatial distribution behaviour is controlled by location errors.

In Figs 13, 14, 15 and 16, location accuracy generally improves over time and in later catalogues it improves as one employs more sophisticated interpretation of seismograms. We see that the range of statistical scale-invariant behaviour is shifted towards smaller distances. In a complete CIT catalogue (Fig. 14) which includes early location results, the implied average error is on the order of 3–5 km. In the later part of the catalogue (Fig. 15), the hypocentral moment's scale-invariant part starts at about 1 km. For the newer catalogues (Figs 16 and 13) the curves' scale-invariant behaviour extends to 0.5 and 0.2 km, respectively. On the other hand, we see that the later catalogues exhibit more fluctuations at larger distances, due probably to aftershock clusters of a few large earthquakes.

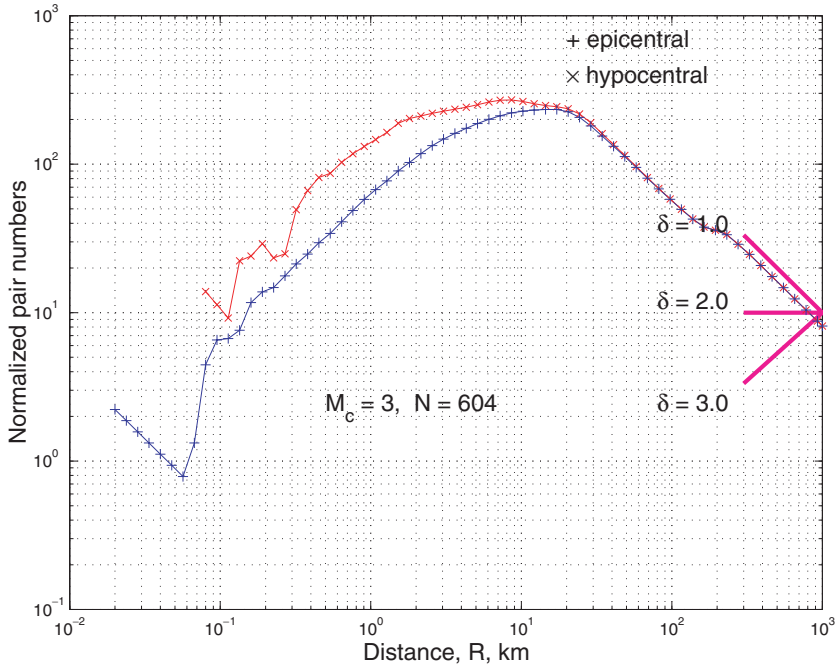

Figure 17. Hypocentral and epicentral spatial moment curves for the southern California (CalTech) catalogue for 1994 ($M_L \geq 3.0$). Same box as in Fig. 1. The upper curve is for the hypocentral moment and the lower for the epicentral.

To demonstrate the influence of the event temporal clustering, in Fig. 17 we show spatial distribution for the year 1994, the year of the Northridge, California earthquake (Thio & Kanamori 1996). The δ_h-dimension for the distance interval 20–200 km is close to 1.0. Most southern California seismicity for this period is concentrated in the Northridge focal zone; hence the scaling dimension for the larger distances is low. For the distance interval 2–20 km, the δ-value is approximately the same as in Figs 14 and 15. This distance range roughly corresponds to the size of the Northridge earthquake rupture zone.

5.3 Global catalogue

Fig. 18 displays epicentral and hypocentral moments for earthquakes in the worldwide PDE catalogue (Section 3) at three depth intervals.

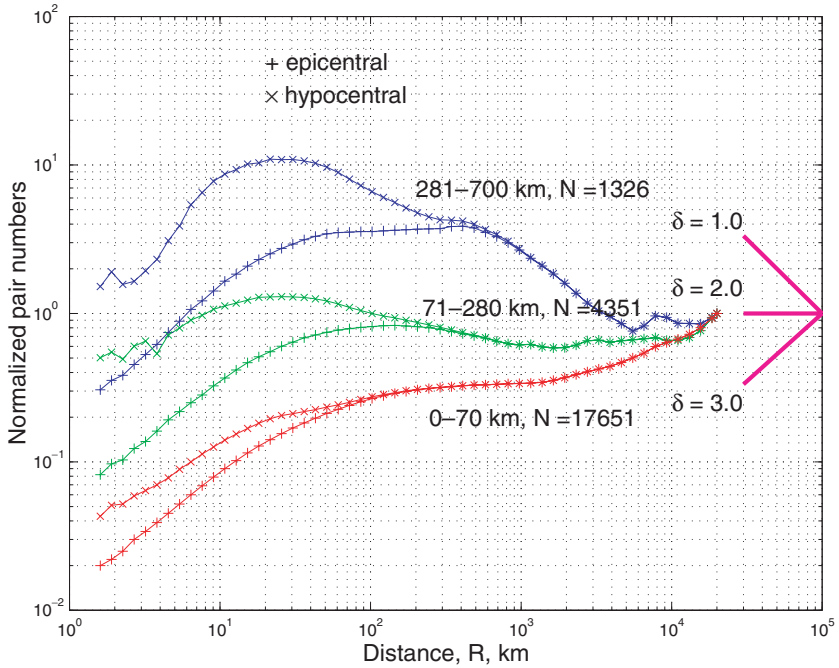

Figure 18. Hypocentral and epicentral spatial moment curves for various depth intervals. The PDE (1965–2003) catalogue with $m_b \geq 5.3$ is used. In each of two curves, the upper one is for the hypocentral moment and the lower for the epicentral. Two upper curves are for the depth interval of 281–700 km; the middle curves are for the depth interval of 71–280 km; and the lower curves are for the depth interval of 0–70 km.

The curves are calculated for the maximum time interval between events (37 yr). We include all pairs of earthquakes without taking the interearthquake time into account.

Similar to (46) we plot the ratio for the epicentral curve

$$N_2^n(R) = \frac{2\,N_2(R)}{N\,(N-1)\,\sin^2\,[R/(2\,R_E)]} \times \frac{R}{\pi\,R_E}, \qquad (47)$$

where R_E is the Earth radius. The hypocentral curve is normalized, using an expression similar to (43).

Epicentral moments yield a higher value of the exponent for distance ranges which are less than, or comparable to, the thickness of the appropriate layer (see Fig. 18). For the hypocentral moment, we normalize the pair numbers by dividing them by the appropriate numbers in a Poisson catalogue in which earthquakes are distributed uniformly over the surface with the same depth distribution as in a real catalogue (Kagan & Knopoff 1978, 1980) (see eq. 43).

Fig. 18 demonstrates that for shallow earthquakes the hypocentral curves are approximately power law in the distance interval 20–2000 km. However, the epicentral curves exhibit a clear transition in their slope at distances corresponding roughly to the thickness of a seismogenic layer. Kagan & Knopoff (1980) showed that the lower distance range of the linearity breakdown (20 km) is explained by location errors, both horizontal and vertical.

The upper cut-off for scale-invariance (2000 km) is connected to the size of major tectonic plates (Kagan & Knopoff 1980; Kagan 1991a). For these distances, statistical self-similarity of the earthquake spatial distribution breaks down.

The δ values in Fig. 18 demonstrate that the dimension decreases as the depth increases. The value of the fractal dimension declines to 1.8–1.9 for intermediate events (depth interval 71–280 km) and to 1.5–1.6 for deeper ones. We see that epicentral and hypocentral curves converge at the distances equal to the thickness of a layer in which earthquakes are selected, the difference between the curves is a consequence of the projection effect and transition from 3-D to 2-D when the distance R increases (Sections 4.3–4.5).

Harte (1998) determined correlation dimensions for shallow and intermediate events in New Zealand. The estimates of the hypocentral correlation dimension (see Table 11.1 in Harte 2001) for deeper earthquakes (1.8–2.2) is slightly higher than for shallow events (1.7–1.9). The larger values of the dimension for intermediate events are, most likely, caused by location errors. As we mentioned in the Introduction, earthquakes registered by seismic networks situated on island chains can have large location errors, and these errors would increase for deeper events. Harte (1998, p. 616; 2001, p. 213) acknowledges that such an explanation is possible.

6 DISCUSSION

Our major thrust has been to analyse errors and systematic effects influencing the estimate of the correlation dimension for spatial earthquake distribution. What can we say about the value of this dimension for the earthquake rupture process? We briefly review attempts to determine the fractal dimension for rock surfaces and earthquake faults.

6.1 Faults and rock surfaces

Ben-Zion & Sammis (2003) show examples of self-similar features of shear fault surfaces (their fig. 3). They also discuss (their Section 2.4) many measurements of scale-invariant features of fault traces, internal fault zone structures and fault networks (see also Kagan 1991a).

Bonnet *et al.* (2001) extensively discuss the properties of fractures at rock surfaces. The fractal dimension of the fault traces at the Earth's surface should be significantly influenced by a free boundary. Moreover, physical properties of the rocks near the surface should differ from rock properties at seismogenic depth. In particular, lithostatic pressure is zero at the surface. Consequently, tectonically stressed rock material would disintegrate, increasing the fractal dimension of the rock particles' distribution.

Schmittbuhl *et al.* (1995) and Amitrano & Schmittbuhl (2002) show that the fractal dimension of rock fracture surfaces is equal to 2.20–2.25. This dimension is determined for one surface. The earthquake fault system contains many fractally distributed surfaces, so their combined dimension may exceed the above value.

Weiss & Marsan (2003) studied spatial distribution of dislocations in an ice crystal. They obtained the correlation dimension estimate of 2.5 ± 0.1 for dislocation clusters, and noticed that close-in-time avalanches are more spatially clustered.

Repeating Mandelbrot's (1983, pp. 103–104) arguments, we suggest that $\delta \geq 2.0$ since any line connecting two blocks of material in shearing motion would intersect at least one fault surface. The dimension of the embedding Euclidean space provides another limit on the value of δ: $3.0 \geq \delta \geq 2.0$. An ideal solid crystal (without defects) would fail along a planar dislocation ($\delta = 2.0$). However, since all natural rocks have defects, this would cause branching and bending of earthquake faults due to fault displacement incompatibility (King 1983; Gabrielov *et al.* 1996). Hence, the fracture correlation dimension would increase.

In general, rock fracture surfaces and exposed faults result from several processes. Hence their fractal dimension may not agree with that for earthquake spatial patterns. In the latter, we directly observe brittle fracturing rocks in situ; therefore, the correlation dimension is relevant to process of rupture. Furthermore, as discussed in Section 4, random and systematic errors of earthquake locations can be approximately evaluated. Such error estimates are more difficult to perform for earthquake faults and rock surface measurements.

6.2 Spatial fractal dimension: monofractal or multifractal?

Is the spatial distribution of earthquakes monofractal or multifractal (Molchan & Kronrod 2005)? In Section 4, we show that practically any value for the correlation dimension can be obtained if many errors and inhomogeneities in the observational data as well as deficiencies in data processing are not properly considered. Presently there are no similar estimates of systematic effects for multifractal measures of the earthquake spatial dimension. Most likely the technical difficulties discussed in Section 4 are intensified for such multifractal measures.

In addition, as we discussed in the Introduction, certain methodological problems must be solved to evaluate multifractal dimensions for hypocentral distributions: the only exponents that have clear physical meaning. Moreover, these estimates need to be obtained for all scale-invariant ranges of spatial earthquake distribution: from distances close to zero to hundreds and thousands of km. Thus, it is doubtful that evaluating multifractal dimensions could yield significant results for presently available catalogues.

Perhaps a better insight into the spatial patterns of earthquake distributions could be obtained by analysing higher order point configurations. Kagan (1981a,b) studied 3- and 4-point spatial moments for earthquake distribution. These moments correspond to point simplexes in 2-D and 3-D, respectively. Similar to the distance between two points, these sets have the advantage of being independent of

any coordinate system and, therefore, lack the problems associated with box counting. The results of these studies suggest that these earthquake distributions are proportional to $1/S$ and $1/V$, where S is the area of a triangle and V is the volume of a tetrahedron formed by earthquake points. These geometrical patterns may provide important information on earthquake generation. A further way to study these multipoint patterns is to use the modern statistical and topological theory of shape (Small 1996; Kendall *et al.* 1999).

6.3 Spatial fractal dimension for earthquake rupture

What are the advantages and drawbacks of using local vs global earthquake catalogues for evaluating the correlation dimension? Local catalogues usually have highly accurate hypocentre solutions. The Hauksson & Shearer (2005) and Shearer *et al.* (2005) catalogue has uncertainties much smaller than the thickness of the seismogenic layer. This high accuracy, as illustrated in Figs 8–9, allows us to directly estimate $\hat{\delta}$ in 3-D and extend the scale-invariant part of the hypocentral moment close to zero distances (see Figs 11–13). However, local catalogues have serious drawbacks: they are often strongly inhomogeneous in time and space. A few aftershock sequences usually dominate the long-range spatial distribution of events, and thus the spatial moment fluctuates strongly at large distances. As the result, $\hat{\delta}$ evaluation becomes difficult. Furthermore, because the high accuracy part of a catalogue is of short span, the $\hat{\delta}$ estimates are strongly influenced by temporal effects.

Global earthquake catalogues have the advantage of more uniform coverage. They have no boundaries, allowing us to study spatial moments for large distances comparable to the Earth's size. However, location uncertainties are much higher in these catalogues compared to local ones. Thus, the moment behaviour at small distances (up to 15–20 km) is controlled by location errors and projection effects. Therefore, the difference between the epicentral and hypocentral moments is small for worldwide catalogues (Fig. 18). However, we can observe scale-invariant behaviour of the moments at a distance range of 20–2000 km and evaluate $\hat{\delta}$. Another advantage of global catalogues is their inclusion of many independent aftershock clusters. Their averaging produces much smoother curves at large distances.

However, in processing global catalogue data, various tectonic regions are combined. Earthquake size statistics are different in these regions (Bird & Kagan 2004), and one may well expect that the spatial distribution pattern also varies. Since earthquakes in subduction zones comprise about 52 per cent of the total (*ibid*), global spatial distributions as in Fig. 18 are largely controlled by subduction earthquakes. In principle, we could subdivide the seismic regions into several categories (*ibid*) and analyse them separately. However, then we would have to work in a relatively constricted distance range between large location errors, specific for global catalogues, and relatively small sizes of tectonic regions.

Comparing spatial moments for various time spans and catalogues yields relevant conclusions about accuracy and the spatial properties of earthquake process. Therefore, we conclude that the statistical self-similarity of earthquake geometry is established down to the scale length of 0.5 km and less. Since the equations of elasticity do not have intrinsic scale, we expect that this property of spatial self-similarity can be extended for the brittle fracture of disordered materials (rocks) up to the scale of a few millimetres: the size of rock grains.

In this paper, we focus on analysing errors and systematic effects to determine the correlation dimension. Even if these biases are taken into account, the actual study of earthquake spatial patterns yields no reliable and converging estimates of the $\hat{\delta}$. Previous investigations (Kagan & Knopoff 1980; Kagan 1991a) suggest that the $\hat{\delta}$-value does not depend or has weak dependence on the magnitude threshold. However, the correlation dimension dependence on catalogue time intervals (see Section 4.7) and the dimension for aftershocks of large earthquakes still need to be explored. Many systematic effects discussed in Section 4 make such investigations difficult.

Our analysis suggests that evaluating the fractal dimension for earthquake spatial patterns is difficult and prone to many errors and biases. This probably explains that in contrast to two other classical statistical scale-invariant exponents of earthquake distribution, the Gutenberg-Richter relation (Bird & Kagan 2004) and Omori's law (Kagan & Houston 2005), which arguably are controlled by universal parameters, or by those with a slight variation, the properties and value of the correlation dimension are not yet agreed upon. We hope that the evidence presented here will persuade readers that the earthquake spatial distribution, at least in asymptotic time limit, has universal features also.

7 CONCLUSIONS

We briefly summarize our results and highlight their difference from similar investigations:

(1) We provide closed-form expressions for most of systematic effects and random errors influencing estimates of the correlation dimension for the earthquake spatial pattern. We test these formulae by simulation.

(2) We evaluate the correlation dimension both for hypocentral and epicentral earthquake patterns and provide algorithms for comparison and mutual transformation of these two dimensions.

(3) We estimate the correlation dimension for several local and global earthquake catalogues. Since these catalogues have different systematic and random biases and errors which influence the correlation dimension estimate, the reported results of the statistical analysis are more robust.

ACKNOWLEDGMENTS

I appreciate partial support from the National Science Foundation through grants EAR 00-01128, EAR 04-09890, and DMS-0306526, as well as from the Southern California Earthquake Center (SCEC). SCEC is funded by NSF Cooperative Agreement EAR-0106924 and USGS Cooperative Agreement 02HQAG0008. The author thanks D. D. Jackson, A. Helmstetter, F. Schoenberg and I. V. Zaliapin of UCLA and D. Vere-Jones of Wellington University for very useful discussions. Agnès Helmstetter helped to construct Figs 8–10. Reviews by David Harte and by two anonymous reviewers have been very helpful in revising the manuscript. I thank Kathleen Jackson for significant improvements in the text. Publication 1033, SCEC.

REFERENCES

Abramowitz, M. & Stegun, I.A., 1972. *Handbook of Mathematical Functions,* Dover, NY, p. 1046.

Aki, K., 1981. A probabilistic synthesis of precursory phenomena, in *Earthquake Prediction, An International Review,* Maurice Ewing Vol. 4, pp. 566–574, eds Simpson, D.W. & Richards, P.G., AGU, Washington, DC.

Amitrano, D. & Schmittbuhl, J., 2002. Fracture roughness and gouge distribution of a granite shear band, *J. geophys. Res.,* **107**(B12), ESE-19, 1–16, Art. No. 2375.

Bak, P., Christensen, K., Danon, L. & Scanlon, T., 2002. Unified scaling law for earthquakes, *Phys. Rev. Lett.,* **88,** 178 501, 1–4.

Ben-Zion, Y. & Sammis, C.G., 2003. Characterization of fault zones, *Pure appl. Geophys.,* **160,** 677–715.

Bird, P. & Kagan, Y.Y., 2004. Plate-tectonic analysis of shallow seismicity: apparent boundary width, beta-value, corner magnitude, coupled lithosphere thickness, and coupling in seven tectonic settings, *Bull. seism. Soc. Am.,* **94**(6), 2380–2399 (plus electronic supplement), see also http://element.ess.ucla.edu/publications/-2004_global_coupling/2004_global_coupling.htm

Bonnet, E., Bour, O., Odling, N.E., Davy, P., Main, I., Cowie, P. & Berkowitz, B., 2001. Scaling of fracture systems in geological media, *Rev. Geophys.,* **39,** 347–383.

Daley, D.J. & Vere-Jones, D., 2003. *An Introduction to the Theory of Point Processes,* 2nd edn, **Vol. 1,** pp. 469, Springer-Verlag, New York.

De Luca, L., Lasocki, S., Luzio, D. & Vitale, M., 1999. Fractal dimension confidence interval estimation of epicentral distributions, *Annali di Geofisica,* **42**(5), 911–925.

De Luca, L., Luzio, D. & Vitale, M., 2002. A ML estimator of the correlation dimension for left-hand truncated data samples, *Pure appl. Geophys.,* **159,** 2789–2803.

Eneva, M., 1996. Effect of limited data sets in evaluating the scaling properties of spatially distributed data: an example from mining-induced seismic activity, *Geophys. J. Int.,* **124,** 773–786.

Fisher, R.A., 1928. General sampling distribution of the multiple correlation coefficient, *Proc. Roy. Soc. Lond, Ser. A,* **121,** 654–673.

Gabrielov, A., Keilis-Borok, V. & Jackson, D.D., 1996. Geometric incompatibility in a fault system, *Proc. Natl. Acad. Sci. USA,* **93,** 3838–3842.

Garwood, F., 1947. The variance of the overlap of geometrical figures with reference to a bombing problem, *Biometrika,* **34,** 1–17.

Geilikman, M.B., Golubeva, T.V. & Pisarenko, V.F., 1990. Multifractal patterns of seismicity, *Earth planet. Sci. Lett.,* **99,** 127–132.

Ghosh, P., 1951. Random distance within a rectangle and between two rectangles, *Bull. Calcutta Math. Soc.,* **43,** 17–24.

Hammersley, J.M., 1950. The distribution of distance in a hypersphere. *Ann. Math. Stat.,* **21,** 447–452.

Harte, D., 1998. Dimension estimates of earthquake epicentres and hypocentres, *J. Nonlinear Sci.,* **8,** 581–618.

Harte, D., 2001. *Multifractals: Theory and Applications,* Boca Raton, Chapman & Hall, 248 pp.

Harte, D. & Vere-Jones, D., 1999. Differences in coverage between the PDE and New Zealand local earthquake catalogues, *New Zealand J. Geol. Geoph.,* **42,** 237–253.

Hauksson, E. & Shearer, P., 2005. Southern California hypocenter relocation with waveform cross-correlation, part 1: results using the double-difference method, *Bull. seism. Soc. Am.,* **95**(3), 896–903.

Hileman, J.A., Allen, C.R. & Nordquist, J.M., 1973. *Seismicity of the Southern California Region, 1 January 1932 to 31 December 1972,* Cal. Inst. Technology, Pasadena.

Helmstetter, A., Kagan, Y.Y. & Jackson, D.D., 2005. Importance of small earthquakes for stress transfers and earthquake triggering, *J. geophys. Res.,* **110**(5), B05S08, doi:10.1029/2004JB003286, pp. 1–13.

Hutton, L.K. & Jones, L.M., 1993. Local magnitudes and apparent variations in seismicity rates in Southern California, *Bull. seism. Soc. Am.,* **83,** 313–329.

Kagan, Y.Y., 1981a. Spatial distribution of earthquakes: the three-point moment function, *Geophys. J. R. astr. Soc.,* **67,** 697–717.

Kagan, Y.Y., 1981b. Spatial distribution of earthquakes: the four-point moment function, *Geophys. J. R. astr. Soc.,* **67,** 719–733.

Kagan, Y.Y., 1982. Stochastic model of earthquake fault geometry, *Geophys. J. R. astr. Soc.,* **71,** 659–691.

Kagan, Y.Y., 1991a. Fractal dimension of brittle fracture, *J. Nonlinear Sci.,* **1,** 1–16. http://moho.ess.ucla.edu/~kagan/1991_Nonlin_science.pdf

Kagan, Y.Y., 1991b. Seismic moment distribution, *Geophys. J. Int.,* **106,** 123–134.

Kagan, Y.Y., 1999. Universality of the seismic moment-frequency relation, *Pure appl. Geophys.,* **155,** 537–573.

Kagan, Y.Y., 2003. Accuracy of modern global earthquake catalogs, *Phys. Earth planet. Inter.,* **135**(2–3), 173–209.

Kagan, Y.Y., 2004. Short-term properties of earthquake catalogs and models of earthquake source, *Bull. seism. Soc. Am.,* **94**(4), 1207–1228.

Kagan, Y.Y. & Houston, H., 2005. Relation between mainshock rupture process and Omori's law for aftershock moment release rate, *Geophys. J. Int.,* **163**(3), 1039–1048.

Kagan, Y.Y. & Jackson, D.D., 1991. Long-term earthquake clustering, *Geophys. J. Int.,* **104,** 117–133.

Kagan, Y.Y. & Knopoff, L., 1978. Statistical study of the occurrence of shallow earthquakes, *Geophys. J. R. astr. Soc.,* **55,** 67–86.

Kagan, Y.Y. & Knopoff, L., 1980. Spatial distribution of earthquakes: the two-point correlation function, *Geophys. J. R. astr. Soc.,* **62,** 303–320.

Kagan, Y.Y., Jackson, D.D. & Rong, Y.F., 2006. A new catalog of southern California earthquakes, 1800–2005, *Seism. Res. Lett.,* **77**(1), 30–38, http://scec.ess.ucla.edu/~ykagan/calif_index.html

Kagan, Y.Y. & Vere-Jones, D., 1996. Problems in the modelling and statistical analysis of earthquakes, in: *Lecture Notes in Statistics,* 114, pp. 398–425, eds Heyde, C.C., Prohorov, Yu. V., Pyke, R. & Racher, S.T. New York, Springer.

Kendall, D.G., Barden, D., Carne, T.K. & Le, H., 1999. *Shape and Shape Theory,* New York, Wiley, pp. 306.

Kendall, M.G. & Moran, P.A.P., 1963. *Geometrical Probabilities,* Hafner, N.Y., 125 pp.

King, G., 1983. The accommodation of large strains in the upper lithosphere of the Earth and other solids by self-similar fault systems: the geometrical origin of *b*-value, *Pure appl. Geophys.,* **121,** 761–815.

Libicki, E. & Ben-Zion, Y., 2005. Stochastic branching models of fault surfaces and estimated fractal dimension, *Pure appl. Geophys.,* **162**(6–7), 1077–1111.

Mandelbrot, B.B., 1983. *The Fractal Geometry of Nature,* 2nd edn, W. H. Freeman, San Francisco, Calif., p. 468.

Marsaglia, G., 1972. Choosing a point from the surface of a sphere, *Ann. Math. Stat.,* **43,** 645–646.

Matheron, G., 1971. *The Theory of Regionalized Variables and its Applications,* Cahiers du Centre de Morphologie Mathematique de Fontainebleau, No. 5., 211 pp.

McCaffrey, R., 1997. Statistical significance of the seismic coupling coefficient, *Bull. seism. Soc. Am.,* **87,** 1069–1073.

Molchan, G. & Kronrod, T., 2005. On the spatial scaling of seismicity rate, *Geophys. J. Int.,* **162**(3), 899–909, doi:10.1111/j.1365–246X.2005.02693.x

Nerenberg, M.A.H. & Essex, C., 1990. Correlation dimension and systematic geometric effects, *Phys. Rev.,* **A42,** 7065–7074.

Ogata, Y. & Katsura, K., 1991. Maximum likelihood estimates of the fractal dimension for random point patterns, *Biometrika,* **78,** 463–474.

Pisarenko, D.V. & Pisarenko, V.F., 1995. Statistical estimation of the correlation dimension, *Phys. Lett. A,* **197,** 31–39.

Preliminary Determination of Epicenters, (PDE), Monthly Listings (1999). U.S. Dept. Interior/Geol. Survey, Nat. Earthquake Inform. Center, January, pp. 47.

Richards, P.G., Waldhauser, F., Schaff, D. & Kim, W.Y., 2006. The applicability of modern methods of earthquake location, *Pure appl. Geophys.,* **163**(2–3), 351–372.

Richards-Dinger, K.B. & Shearer, P.M., 2000. Earthquake locations in southern California obtained using source-specific station terms, *J. geophys. Res.,* **105**(B5), 10 939–10 960.

Ripley, B.D., 1988. *Statistical Inference for Spatial Processes,* Cambridge University Press, Cambridge, 148 pp.

Schmittbuhl, J., Schmitt, F. & Scholz, C., 1995. Scaling invariance of crack surfaces, *J. geophys. Res.,* **100**(4), 5953–5974.

Shearer, P., Hauksson, E. & Lin, G.Q., 2005. Southern California hypocenter relocation with waveform cross-correlation, part 2: results using source-specific station terms and cluster analysis, *Bull. seism. Soc. Am.,* **95**(3), 904–915.

Small, C.G., 1996. *The Statistical Theory of Shape,* Springer, New York, pp. 227.

Smith, L.A., 1988. Intrinsic limits on dimension calculations, *Phys. Lett. A,* **133,** 283–288.

Stoyan, D. & Stoyan, H., 1994. *Fractals, Random Shapes, and Point Fields: Methods of Geometrical Statistics,* Wiley, New York, pp. 389.

Thio, H.K. & Kanamori, H., 1996. Source complexity of the 1994 Northridge earthquake and its relation to aftershock mechanisms, *Bull. seism. Soc. Am.,* **86,** S84–S92.

Vere-Jones, D., 1999. On the fractal dimensions of point patterns, *Adv. Appl. Probab.,* **31,** 643–663.

Vere-Jones, D., Davies, R.B., Harte, D., Mikosch, T. & Wang, Q., 1997. Problems and examples in the estimation of fractal dimension from meterological and earthquake data, in *Proc. Int. Conf. on Application of Time Series in Physics, Astronomy and Meteorology,* pp. 359–375, eds Subba Rao, T., Priestley, M.B. & Lessi, O., Chapman & Hall, London.

Weiss, J. & Marsan, D., 2003. Three-dimensional mapping of dislocation avalanches: clustering and space/time coupling, *Science,* **299,** 89–92.

Wiemer, S. & Wyss, M., 2000. Minimum magnitude of completeness in earthquake catalogs: examples from Alaska, the western United States, and Japan, *Bull. seism. Soc. Am.,* **90,** 859–869.

Wolfram, S., 1999. *The Mathematica Book,* 4th edn, Champaign, IL, Wolfram Media, Cambridge, New York, Cambridge University Press, pp. 1470.

Wyss, M., Sammis, C.G., Nadeau, R.M. & Wiemer, S., 2004. Fractal dimension and *b*-value on creeping and locked patches of the San Andreas fault near Parkfield, California, *Bull. seism. Soc. Am.,* **94,** 410–421.